https://doi.org/10.5194/egusphere-2026-1525
Preprint. Discussion started: 30 April 2026

Characterizing melt ponds on sea ice in the Norwegian Earth System Model (NorESM2)

Caixin Wang caixin.wang@met.no[1], Jens Debernard [1], and Keguang Wang [1]
[1]Norwegian Meteorological Institute, Henrik Mohns plass 1, 0371, Oslo, Norway

Abstract. Melt Ponds (MPs) are pools of open water that formed on Arctic sea ice during the warm months. They significantly affect the surface radiation budget of the Arctic Ocean and play an important role in the Arctic sea ice mass balance, climate and ecological systems. The second generation of the coupled Earth System Model developed by the Norwegian Climate Center, NorESM2, includes an explicit representation of MPs. To characterize the spatial distribution and the seasonal evolution of MPs, we introduced four key variables: melt pond fraction (MPF), relative melt pond fraction (RMPF), MP area (MPA), and pond area fraction (PAF). Using these variables, particularly PAF, we conducted a comprehensive evaluation of MPs in NorESM2 across the Pan-Arctic region and its four sub-regions: the Pacific, Atlantic, Laptev and Canadian sector. Additionally, we classified MPs base on ice type, distinguishing between first-year ice (FYI) and multi-year ice (MYI), over the period from May to September during 2002-2011. This study utilized observational data, including MPF from MODIS and MERIS, sea ice age from NSIDC, sea ice concentration from MODIS and AMSR-E, and surface downward solar radiation from SYN1deg, and reanalysis atmospheric data from ERA5. Our study revealed that while differences existed between MODIS and MERIS, these discrepancies were relatively small during May, June and September, which corresponds to the early melt season and the refreezing season. In contrast, larger discrepancies were observed during July and August, the peak melt season. These significant deviations are likely attributed to the challenges associated with retrieving MPF using coarse-resolution optical sensors. Despite these differences, the overall spatial patterns and temporal evolutions of MPs derived from MODIS and MERIS were largely consistent. MPs were found to form earlier and more extensively on FYI compared to MYI, leading to more abundance of MPs on FYI. NorESM2 successfully reproduced these general characteristics. However, the model consistently simulated the maximum PAF was in August (except for FYI in the Pacific region), which was typically one month later than in the observations. NorESM2 exhibited a systematic underestimation of MPs in May and June, not only in the pan-Arctic but also across the sub-regions, and on both FYI and MYI. Conversely, MPs on MYI in the Pacfic sector were overestimated, likely due to the higher prevalence of MYI in NorESM2 during these months in this region. The systematic underestimation of MPs in NorESM2 during the early melt season can be attributed to the too low surface downward solar radiation in NorESM2 and the too large retrieved MPF from MODIS and MERIS. The former attribution was further confirmed by the experiments conducted with the 1D sea ice model ICEPACK. Giving the critical role of MPs play in Arctic albedo and energy budgets, advancing the representation of MPs in the model has a profound implications for the Arctic system.

https://doi.org/10.5194/egusphere-2026-1525
Preprint. Discussion started: 30 April 2026

1 Introduction

Arctic sea ice is a barrier between the Arctic atmosphere and ocean in exchanging heat, moisture and momentum. It plays a critical role in regulating regional oceanic and global climate conditions and is often considered to be one of the most sensitive indicators of Earth's climate change. The Arctic sea ice in recent decades has been undergoing dramatic decrease in sea ice area, extent, thickness and volume (e.g., Comiso et al. 2008; Kwok and Rothrock 2009; Stroeve et al. 2012; Kacimi and Kwok 2022; Lindsey and Scott 2022; Meier and Stroeve 2022; Wang et al. 2022), in particular in September with the strongest sea ice extent decrease of -13.4% per decade between 1979 and 2021 (C3S, 2022). As a result, the ice pack is becoming more and more dominated by first-year ice (FYI) (Nghiem et al., 2007; Maslanik et al., 2011; Meier and Stroeve, 2022). With the continuous decrease of the Arctic sea ice, an ice-free Arctic could appear at earliest in the 2020s to 2030s, or are likely going to occur by 2050 (Notz and Community, 2020; Bonan et al., 2021; Heuzé and Jahn, 2024). The large uncertainties of the predictions of ice-free Arctic depend on the definition of ice-free, model bias, internal variability and external forcing (Kim et al., 2023; Topál and Ding; Jahn et al., 2024).

The decrease of Arctic sea ice reduces the surface albedo and allows more solar radiation absorbed by the upper ocean (Perovich et al., 2007, 2008), thereby enhancing ice melt and contributing to further ice decline (Steele et al., 2010; Serreze and Stroeve, 2015). This ice-albedo feedback is further enhanced by the presence of melt ponds (MPs), since MPs have lower albedo than un-ponded ice (e.g., Hanesiak et al. 2001; Perovich et al. 2002a; Perovich and Polashenski 2012; Tao et al. 2024). The decreased surface albedo owing to MPs leads to more solar radiation absorbed by the upper ocean, thus enhancing upper ocean warming, favoring sea ice melting and promoting more primary production within and beneath the sea ice (Light et al., 2008; Nicolaus et al., 2012; Katlein et al., 2019; Horvat et al., 2020; Diamond et al., 2021). MPs thus play a critical role in the mass balance of Arctic sea ice and the climate and eco- system (Flocco et al., 2012; Holland et al., 2012; Hunke et al., 2013; Schröder et al., 2014). With the thinning of the Arctic sea ice, MPs are believed to be a reliable predictor for the summer sea ice conditions (Schröder et al., 2014; Liu et al., 2015; Diamond et al., 2021).

Most of our knowledge on MPs is from in-situ observations and/or remote sensing measurements or more recently from Artificial Intelligence (AI) techniques. The in-situ observations can provide accurate and precise local measurements of MPs, but collection of in-situ MPs data in the Arctic is costly, restricted, and has limited spatial coverage due to the harsh environment, dynamic nature of the sea ice and accessibility to the Arctic. Satellite remote sensing measurements cover larger areas of the Arctic, but it often sacrifices resolution and relies on ground measurements. For example, the optical sensors, MODIS (Moderate Resolution Image Spectroradiometer), MERIS (Medium Resolution Imaging Spectrometer), and Sentinel-2, Sentinel-3 and Landsat 8, are widely used, especially the first two, to retrieve melt pond fraction (MPF) due to their capacity to measure the spectral reflectance from open water, sea ice and MPs. But the coarse resolution and optical property of these sensors lead to the challenges in discriminating small open waters, leads and MPs. Laser altimeter, such as ICESAT-2 (the Ice, Cloud, and land Elevation Satellite-2), has a high resolution and can provide detailed melting condition on sea ice surfaces. It has been

https://doi.org/10.5194/egusphere-2026-1525
Preprint. Discussion started: 30 April 2026

used to retrieve MPs recently (e.g., Buckley et al. 2023), but only regional or short period products are available. AI, also namely machine learning and deep learning, is another technique to identify MPs. It relies on large amount of high-quality data. Consequently, each approach has its own advantages and shortcomings as discussed by Aparício (2023).

MPs are pools of open water on Arctic sea ice during the late spring and summer due to the accumulation of rain water or snow/ice meltwater (Perovich et al., 2002a; Polashenski et al., 2012; Webster et al., 2015, 2022; Buckley et al., 2023). The evolution and distribution of MPs are affected by the physical properties of sea ice, such as surface topography, surface roughness, ice morphology (Eicken et al., 2002, 2004; Polashenski et al., 2012; Webster et al., 2015; Buth et al., 2025; Fuchs et al., 2025). It is also found there is a strong geometric correlation between warm anomalies in winter which are associated with thinner snow and ice and melt pond location in the following summer (Thielke et al., 2023). The evolution of MPs is generally characterized by four stages (Eicken et al., 2002; Perovich and Polashenski, 2012; Polashenski et al., 2012; Webster et al., 2015; Ding et al., 2020). Due to the differences of physical properties and ice permeability between FYI and multi-year ice (MYI), the evolution of MPs on FYI and MYI are quite different. In the first stage when the pond starts to form, ponds on MYI tend to be confined to deeper pools with less spatial coverage, while ponds on FYI tend to be shallower but more widespread due to limited relief on FYI (Morassutti and LeDrew, 1996; Hanesiak et al., 2001). In the second stage when pond drains (which usually occurs within a few days), the pond coverage drops substantially on FYI, but only slightly on MYI. In the third stage, the pond evolves on ice, with pond coverage on both FYI and MYI increasing steadily, and often reaching its seasonal maximum. During this stage, ponds may melt through to the ocean and the ice may melt entirely. In the final stage, ponds on FYI and MYI start to refreeze, with a thin layer of ice forming on ponds. This can happen whenever the changing atmospheric forcing results in freezing conditions during the season. MPs lower the surface albedo of sea ice (Eicken et al., 2004), causing the FYI to have an even more smaller albedo than MYI (Perovich and Polashenski, 2012), which result in more solar radiation absorption in the upper-ocean underneath FYI than MYI (Nicolaus et al., 2013; Lei et al., 2016), and consequently more under-ice phytoplankton bloom under FYI (Arrigo et al., 2012).

MPs play an important role in the climate and biological system. They contribute significantly to the simulated loss of summer sea ice through reducing the albedo (Diamond et al., 2021), and tend to increase bottom and lateral melt by allowing more sunlight to penetrate through the ponded ice cover (Zhang et al., 2018; Keen et al., 2021). Inclusion of MPs in models is therefore important for accurate simulation of sea ice in models. There has been increasing efforts to implicitly or explicitly incorporate MPs into large-scale climate and operational forecast models (Flocco et al., 2010; Holland et al., 2012; Hunke et al., 2013; Webster et al., 2022). For example, of the 125 CMIP6 model configurations, 111 models implicitly while 14 models explicitly incorporate MPs schemes (Aparício, 2023). The choice of MP scheme may affect the amount of basal growth, basal melt and top melt (Keen et al., 2021). Consequently, the employed MP schemes have significant impacts on the simulated Arctic sea ice and climate (Holland et al., 2012; Keen et al., 2021), especially under warmer climates (Diamond et al., 2024). NorESM2 (the Norwegian Earth System Model version 2) is one of the 14 CMIP6 members explicitly incorporating MPs schemes. This model is an important tool for Norwegian climate researchers in the study of past, present and future climate. It has been thoroughly evaluated by Seland et al. (2020) regarding the stability of the pre-industrial climate and the sensitivity of the model to abrupt and gradual quadrupling of CO_2 as well as the ability of the model to simulate the historical climate

https://doi.org/10.5194/egusphere-2026-1525
Preprint. Discussion started: 30 April 2026

under the CMIP6 forcings. It has also been evaluated together with other CMIP6 models regarding the simulation of Arctic sea ice. For example, Notz and Community (2020) examined the CMIP6 simulations of the Arctic sea ice area and volume over the period 1979-1998, Henke et al. (2023) accessed the Arctic sea ice thickness and area during 1979-2014, Keen et al. (2021) inter-compared the mass budget of the Arctic sea ice for the period of 1960-2100. However, how representation of MPs in the model remains unclear yet. In this study, through comparison with two retrieved MPF dataset, the representation of the MPs in NorESM2 is thoroughly evaluated during the period of 2002-2011 in Section 3. In addition, the influencing of downward surface solar radiation (DSR) on MPs formation is further investigated with the 1D sea ice model ICEPACK in Section 4. Models, data and methodology used in this study are introduced in Section 2.

2 Models, data and methodology

2.1 Models

2.1.1 NorESM2

NorESM2 is the second generation coupled Earth system model (ESM) based on the Community Earth System Model (CESM2.1) developed by the Norwegian Climate Center (Danabasoglu et al., 2020). It is the successor of NorESM1 (Bentsen et al., 2013), and is a member of CMIP6 (Coupled Model Inter-comparison Project Phase 6) (Eyring et al., 2016; Seland et al., 2020). NorESM2 consists of atmosphere, ocean, ocean biogeochemistry, sea ice, land, and river, as well as a coupler.

The sea ice component in NorESM2 is the Los Alamos sea ice model (CICE5.1.2) (Hunke et al., 2015), which simulates the growth, melt, movement and deformation of sea ice. It includes an elastic-viscous-plastic (EVP) rheology dynamics (Hunke and Dukowicz, 1997), a mushy-layer thermodynamics (Turner and Hunke, 2015), a Delta-Eddington radiative transfer scheme (Briegleb and Light, 2007), and considers the effects of wind drift of snow into the ocean following Lecomte et al. (2013). The MPs scheme employs the level-ice MP parameterization (Hunke and Lipscomb, 2010), in which the ponds evolve according to physical-based process descriptions, assuming a thickness-area ratio for changes in pond volume (Hunke et al., 2013). NorESM2 uses the standard five ice thickness categories (Bitz et al., 2001; Lipscomb, 2001), and is configured with eight layers of ice and three layers of snow.

There are two versions of NorESM2, NorESM2-LM and NorESM2-MM, with the same horizontal resolution (1°) for the ocean and sea ice models, but different horizontal resolution for the atmosphere and land components (2° for NorESM2-LM and 1° for NorESM-MM) (Seland et al., 2020). NorESM2-MM produces a colder ocean and a thicker sea ice in the Arctic compared to NorESM2-LM (Seland et al., 2020). The excessive sea ice in September in NorESM2-MM (Seland et al., 2020) leads us to use only NorESM2-LM in this study. The historical experiments of NorESM2-LM from three ensemble members r1i1p1f1, r2i1p1f1, r3i1p1f1 are employed in this study, where r1i1p1f1, r2i1p1f1 and r3i1p1f1 are variant_labels for CMIP6 data, with r, i, p, and f being the indices for realization, initialization, physics, and forcing.

https://doi.org/10.5194/egusphere-2026-1525
Preprint. Discussion started: 30 April 2026

2.1.2 ICEPACK

ICEPACK is the column version of CICE, representing crucial sea ice processes including thermodynamics, ridging, biogeochemistry, and associated area and thickness changes. It was separated from the CICE after CICE v5.1.2 was released, and maintained by the CICE Consortium (https://github.com/CICE-Consortium/Icepack). ICEPACK has been recently used to study, e.g., the role of the warm Atlantic Water on the sea ice melt north of Svalbard (Duarte et al., 2020) and to reproduce ice mass balance buoy observations in landfast ice (Plante et al., 2024). Utilizing the same configuration as the CICE in NorESM2, the latest version of ICEPACK1.5.0 is used here to study factors influencing the MPs formation.

2.2 Data

2.2.1 Melt pond fraction (MPF)

The MPF data used for the evaluation are from optical satellites MODIS and MERIS. The MODIS MPF data is an 8-day composite developed using the MODIS MOD09A1 weekly surface reflectance data with an Artificial Neural Network (ANN) approach (Rösel et al., 2012, 2015), covering the years 2000-2011 from 9 May to 13 September. MODIS captures the temporal and spatial variability of the MP area well and is often used for calibration and validation (e.g., Zhang et al. 2018; Lee et al. 2024). The MERIS MPF data is daily, originally developed by Zege et al. (2015) and Istomina et al. (2015) based on the newly developed optical model of sea ice reflection, and improved by Istomina and Spreen (2020) and Istomina et al. (2025). It uses the channels of MERIS radiometer on ENVISAT (Environmental Satellite) with the Melt Pond Detector (MPD) algorithm and covers the years of 2002-2011 from 1 May to 30 September. The new version 1.7 of MERIS (Istomina et al., 2025) is used here. Both the MODIS MPF and MERIS MPF have a spatial resolution of 12.5 km. It is noteworthy that the MODIS MPF is defined as a fraction of melt pond per grid cell, while the MERIS MPF is defined as a fraction of melt pond per ice area.

2.2.2 Sea ice age

The National Snow and Ice Data Center (NSIDC)'s EASE-Grid sea ice age data (version 4) (Tschudi et al., 2019) is used to categorize sea ice types (FYI and MYI). It is a weekly data covering the period of January 1984 through December 2019 (https://nsidc.org/data/nsidc-0749) with a spatial resolution of 12.5 km. It categorizes the sea ice as first-year ice (0-1 years old), second-year ice (1-2 years old), and so forth based on how many summer melt seasons the ice has survived. Sea ice age over 1-year is classified as MYI here.

2.2.3 Sea ice concentration

AMSR-E (Advanced Microwave Scanning Radiometer for EOS) SIC was calculated using the ARTIST Sea ice (ASI) algorithm (Spreen et al., 2008), and used to provide the sea ice coverage when deriving the MERIS MPF (Istomina et al., 2025). It is a daily product covering the period June 2002 to December 2011. In addition to the MPF, MODIS also provides open water fraction (OWF) products. Therefore, SIC can be directly obtained from MODIS OWF through 1–OWF, which has the same

https://doi.org/10.5194/egusphere-2026-1525
Preprint. Discussion started: 30 April 2026

8-day interval as MPF data. Since microwaves cannot reliably discriminate open water, MPs on ice floes, leads and openings between ice floes during summer, there are rarely SIC products providing accurate measurements of the summer SIC (Kern et al., 2020).

2.2.4 ERA5

ERA5 is the fifth generation ECMWF atmospheric reanalysis of the global climate, replacing the ERA-Interim reanalysis which stopped on 31 August 2019. ERA5 assimilates and processes the best available observation data from satellites and in-situ stations using ECWMF's Integrated Forecast System (IFS) Cycle 41r2 (Hersbach et al., 2018), and provides data at a considerably higher spatial (31 km) and temporal resolution (hourly) than its legacy counterpart ERA-Interim. It covers the period from 1940 to present. Although ERA5 still has a warm bias as ERA-Interim, it reduces the anomalous Arctic rainfall in ERA-Interim over the Arctic sea ice (Wang et al., 2019). The reanalysis product of hourly wind at 10 m height, surface air temperature at 2 m height (T2M), total precipitation, specific humidity, surface downward solar radiation (DSR) and surface downward longwave radiation are used to force ICEPACK and to investigate how the DSR influence the MPF.

2.2.5 SYN1deg

SYN1deg, the Synoptic Radiative Fluxes and Clouds products, is one of the products of CERES (the Clouds and the Earth's Radiant Energy) which is a satellite-based data set for the Earth's radiation budget from the top of the atmosphere to the Earth's surface. Its surface products are computed through combination of CERES measured fluxes and atmospheric profiles, ozone, aerosols, cloud cover properties and atmospheric state from satellites or reanalysis. SYN1deg offers data from March 2000 onward with a spatial resolution of 1^ox1^o, and a temporal resolution varying from hourly, daily to monthly. The monthly data of surface DSR during 2002-2011 are used here.

2.3 Methodology

For consistency, May to September during 2002-2011 were chosen as the study period here. The MODIS grid is chosen as the standard, and all the other data are interpolated to the MODIS grid. The results from NorESM2 are monthly. For comparison, the monthly mean observations are calculated from the daily, weekly or 8-day data. As already known, the MODIS MPF data lasts until mid-September, and the MERIS MPF data was obtainable until the last day of September. Since the MPF starts to decrease in autumn with MPs refreezing (Rösel and Kaleschke, 2011; Perovich and Polashenski, 2012), we assume a zero MPF after mid-September for MODIS, thus providing an estimate for the possible lowest MPF in September, namely MODIS-Low. On the other hand, the MODIS data until mid-September offers an estimate of the highest MPF in this month, namely MODIS-High.

MPF is an important parameter for describing MPs and has been widely used in the previous studies (e.g., Rösel et al., 2012; Polashenski et al., 2012; Webster et al., 2015). It has different definitions in the literature, namely, the melt pond fraction per grid cell (Rösel et al., 2012), or the fraction of melt pond relative to the sea ice per grid cell (Li et al., 2020; Istomina et al.,

https://doi.org/10.5194/egusphere-2026-1525
Preprint. Discussion started: 30 April 2026

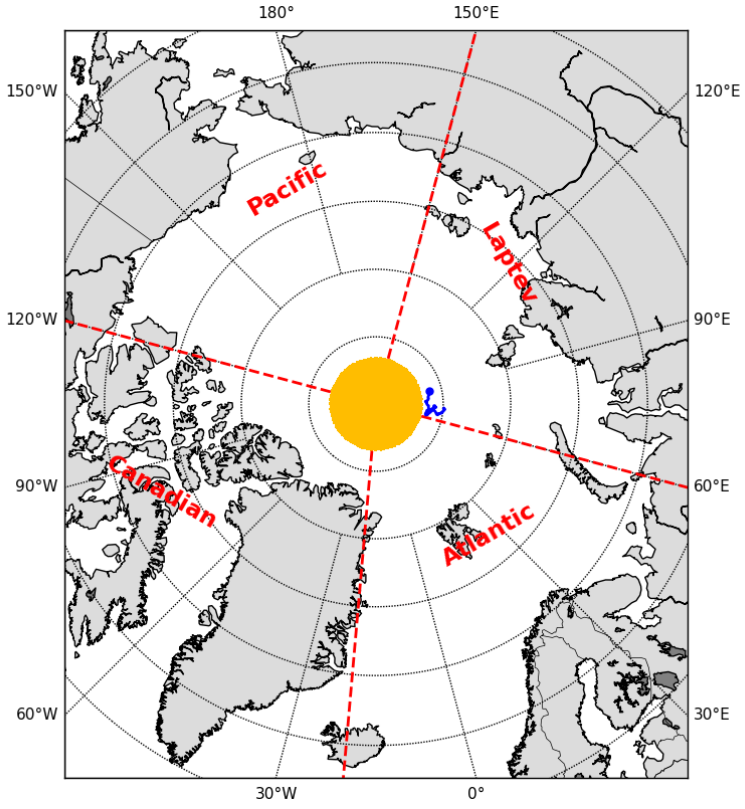

Figure 1. Sub-regions of Atlantic ($20^oW - 60^oE$), Laptev ($60^oE - 150^oE$), Pacific ($150^oE - 120^oW$) and Canadian ($20^oW - 120^oW$). The yellow region (north of $86.5^\circ N$) is masked due to no MERIS MPF data. The solid blue line is the trajectory of IMB buoy of 2004B during the simulation period with circle showing the simulation starting in section 4.2.

2025). The former refers to MPF and the latter refers to relative melt pond fraction (RMPF) in this study such that

$$RMPF = \frac{MPF}{SIC} \tag{1}$$

where MPF and RMPF are all in the range of 0 and 1. MPF is the direct product of MODIS and NorESM2, and RMPF is the direct product of MERIS. The MODIS RMPF and NorESM2 RMPF are calculated using their own SIC, and the MERIS MPF is computed with AMSR-E SIC according to Eq. (1). In addition to MPF and RMPF, we define MP area (MPA), the total area covered by ponds as

$$MPA = \sum MPF \times S \tag{2}$$

which is the sum of MPF multiplying by grid-cell area S covered by sea ice in a domain. Similarly, we define,

$$PAF = \frac{MPA}{SIA} \tag{3}$$

https://doi.org/10.5194/egusphere-2026-1525
Preprint. Discussion started: 30 April 2026

PAF is a ratio, representing the pond area relative to the sea ice area (SIA) in a domain. The deficiency of microwave satellites discriminating between open water/leads and ice may result in large uncertainty in the derived SIC when the SIC is low. To reduce uncertainty, a filter was applied to MPF, RMPF, MPA, and PAF to exclude cases where SIC is less than 0.1. Same SIC cutoff was applied to NorESM2 data when using/calculating MPF, RMPF, MPA and PAF. There is no MPF observation data near the North Pole in MERIS and MODIS, thereby the pole hole north of 86.5°N is excluded during the calculations ((shade area with yellow in Fig. 1). The MPA and PAF are further investigated in four subdivision regions : the Atlantic sector (20°W - 60°E), the Laptev sector (60°E - 150°E), the Pacific sector (150°E - 120°W), and the Canadian sector (20°W - 120°W). Through classifying PAF on FYI and MYI, the PAF are explored in the Pan-Arctic and the three regions of Pacific, Atlantic and Laptev. An ensemble mean of NorESM2 is calculated from the three ensemble members above (see section 2.1.1) to see the uncertainty of the model. To further explore the performance of the model, several metrics are used in this study, including a multi-year seasonal mean from May to September $\overline{X}$, which is calculated,

$$\overline{X} = \frac{1}{(y_2 - y_1 + 1) * (m_2 - m_1 + 1)} \sum_{j=y_1}^{y_2} \sum_{i=m_1}^{m_2} X_{i,j} \tag{4}$$

where X are the observations from MODIS or MERIS, or the results from NorESM2, i represents months from May (m_1) to September (m_2), and j demotes years from 2002 (y_1) to 2011 (y_2). Bias indicates the difference between the model and the observation, which is calculated as,

$$Bias = \hat{f}(x) - f(x) \tag{5}$$

where $\hat{f}(x)$ is the model results from NorESM2 and $f(x)$ are the observations from MODIS or MERIS. Negative values indicate underestimation and positive values suggest overestimation. To further measure the difference between NorESM2 and observations, the relative error (RE) is defined as,

$$RE = \frac{Bias}{f(x)} \times 100\% \tag{6}$$

and the root mean square error is,

$$RMSE = \sqrt{\sum_{i=1}^{n} \frac{(\hat{f}(x_i) - f(x_i))^2}{n}} \tag{7}$$

and the standard deviation is,

$$STD = \sqrt{\sum_{i=1}^{n} \frac{(\hat{f}(x_i) - \overline{\hat{f}(x_i)})^2}{n}} \tag{8}$$

3 Results

3.1 Spatial distributions of MPs

Figure 2 shows the spatial distributions of monthly mean MPF as observed by MODIS, MERIS and simulated by NorESM2 from May to September during the period 2002-2011. The observations clearly showed the seasonal progression of MPs,

https://doi.org/10.5194/egusphere-2026-1525
Preprint. Discussion started: 30 April 2026

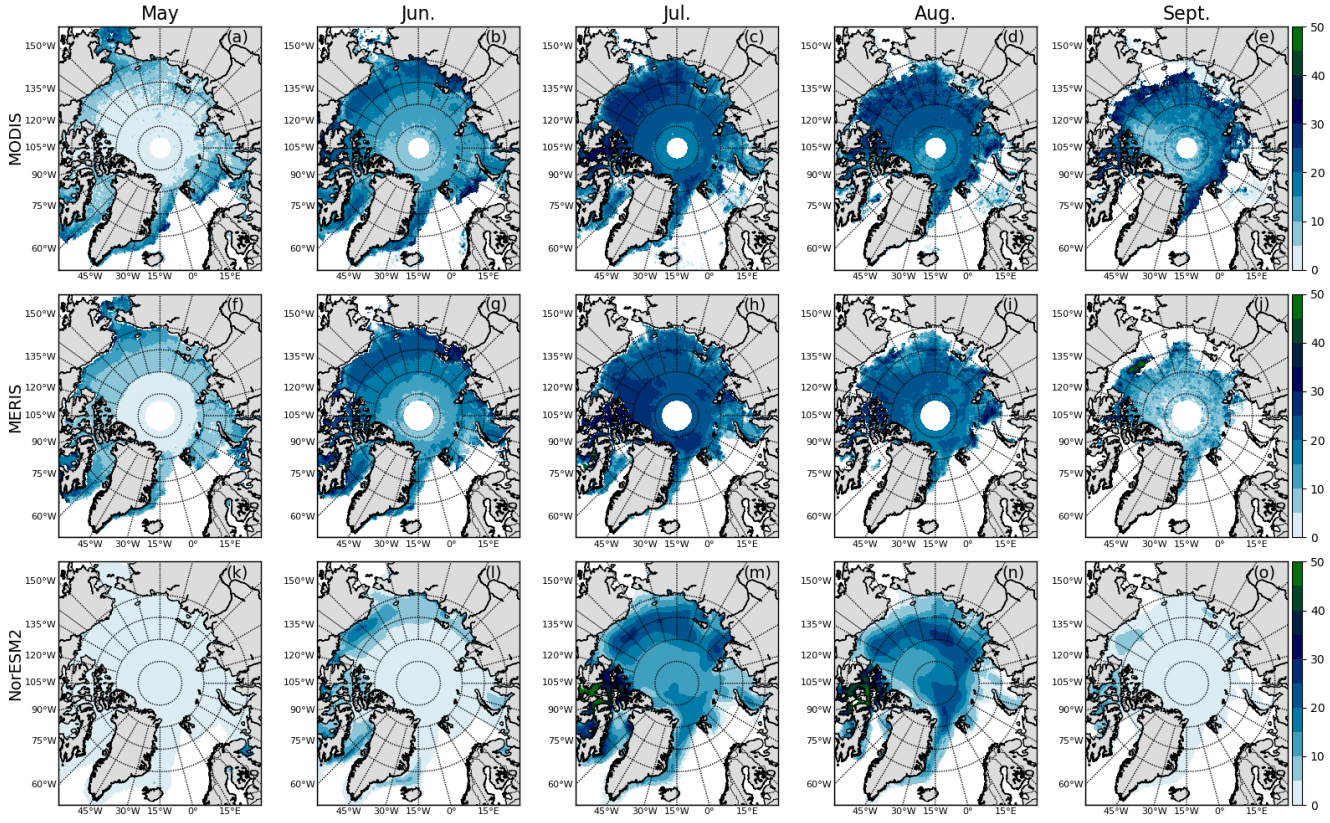

Figure 2. Spatial distributions of monthly mean MPF in MODIS (a-e), MERIS (f-j), and NorESM2 (k-o) in May (a, f, k), June (b, g, i), July (c, h, m), August (d, i, n), and September (e, j, o) over the period of 2002-2011. Similarly, MODIS-High was used here.

beginning in the southern latitudes near the ice edge during spring and gradually extending northward in summer. When the MPs in the northern latitudes refrozen or disappeared in autumn, there were still MPs in the southern latitudes. In May, the MPF was mostly less than 20% in MODIS and MERIS when the MPs started to develop near the southern ice edge (Fig. 2a & 2f). In June, the MPs in the southern latitudes further developed, with the MPF usually being 20-30%; During this time, they started to form in the northern latitudes (Fig. 2b & 2g). In July, the MPF of 20-30% covered most of the Arctic ocean except near the North Pole where the MPF was 15-20% in MODIS and 20-25% in MERIS (Fig. 2c & 2h). The MPF over 30% was mainly found in the Canadian bays/straits. From August, although the MPF in the southern latitudes remained around 20-30%, it started to decrease with the MPs starting to refreeze in the northern latitudes (Fig. 2d & 2i). In September, the MPF was still 10-20% over most of the Arctic Ocean, and the MPF of 20-30% could only be found near the ice edge in the southern latitudes (Fig. 2e & 2j).

The MPF in NorESM2 in May was less than 5% over most of the Arctic Ocean, considerably lower than those in MODIS and MERIS (Fig. 2k vs. Fig. 2a & 2f). Although the MPF in NorESM2 increased in June (up to 25%), it was still apparently lower

https://doi.org/10.5194/egusphere-2026-1525
Preprint. Discussion started: 30 April 2026

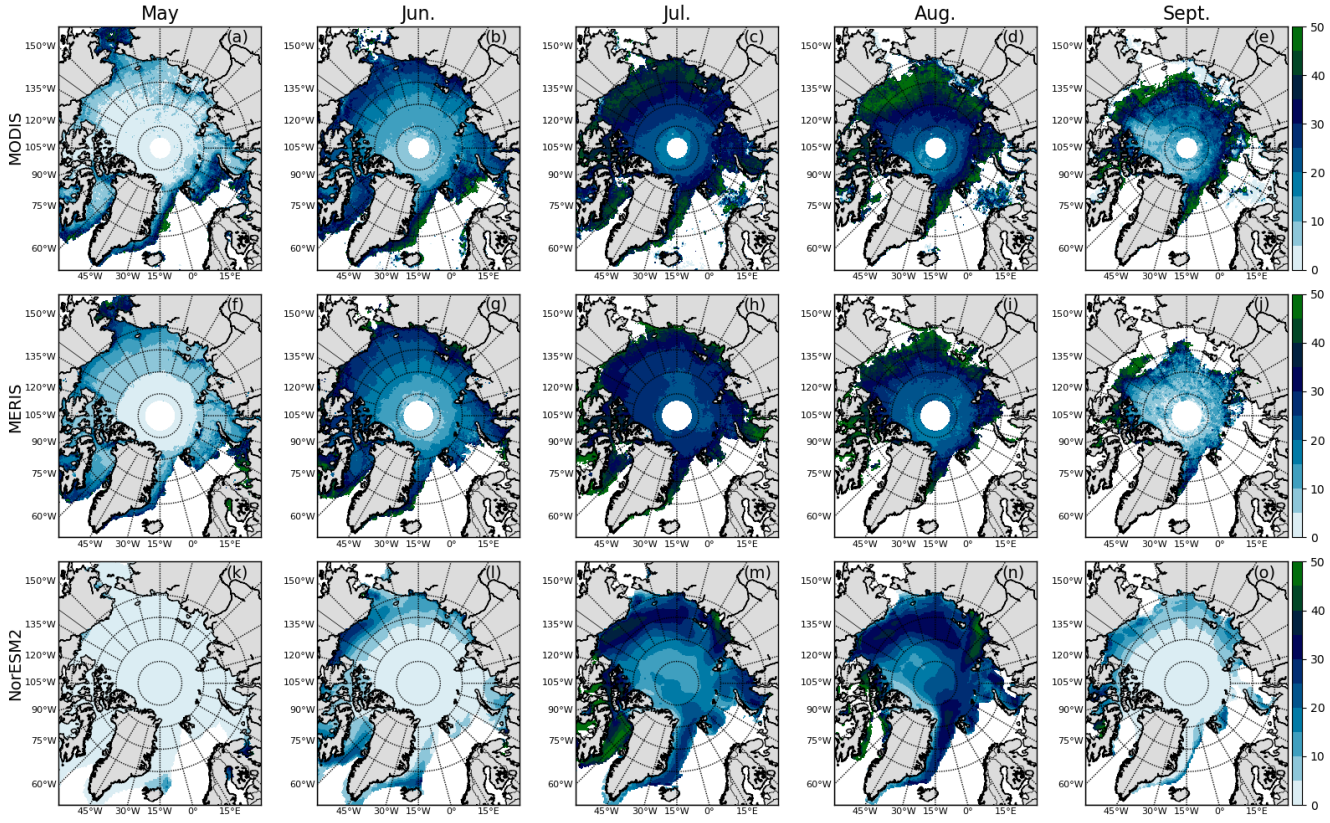

Figure 3. Same as Fig.3, but for RMPF.

than in MODIS and MERIS over most part the Arctic Ocean. In July and August, the NorESM2 MPF was more comparable with those in MODIS and MERIS (Fig. 2c-d vs. Fig. 2h-i, Fig. 2m-n). However, the MPF of 20-30% in NorESM2 in July was mostly found in the Southern latitudes in the Pacific and Laptev regions, while they were largely found in the same regions in MODIS but in the regions of north of Greenland and Canadian Archipelago in MERIS which belong to the Pacific and Canadian regions. In addition, the MPF in NorESM2 was obviously lower near the north pole and north of Greenland and apparently higher in the Canadian bays/straits than those in MODIS and MERIS in July. In August, the similarly lower MPF in NorESM2 was found north of Greenland and near the north Pole. In September, the MPF magnitudes over the Arctic Ocean were much lower than in MODIS and MERIS again (Fig. 2o vs. Fig. 2e & 2j), with the MPF mostly less than 5% (Fig. 2o). The NorESM2 MPF was found in a relatively larger area than those in MODIS and MERIS, in particular in the east of Greenland of the Atlantic region, and in the marginal seas of the Pacific region and in the straits of the Canadian region.

The spatial distributions of RMPF were similar to those of MPF (Fig. 3 vs. Fig. 2), although the RMPF was by definition not smaller than the MPF as shown in Eq. (1). Similar to the MPF, the RMPF in NorESM2 was also notably lower in May, June, and September compared to those in MODIS and MERIS, and agreed better in July and August. In July, the RMPF reached

https://doi.org/10.5194/egusphere-2026-1525
Preprint. Discussion started: 30 April 2026

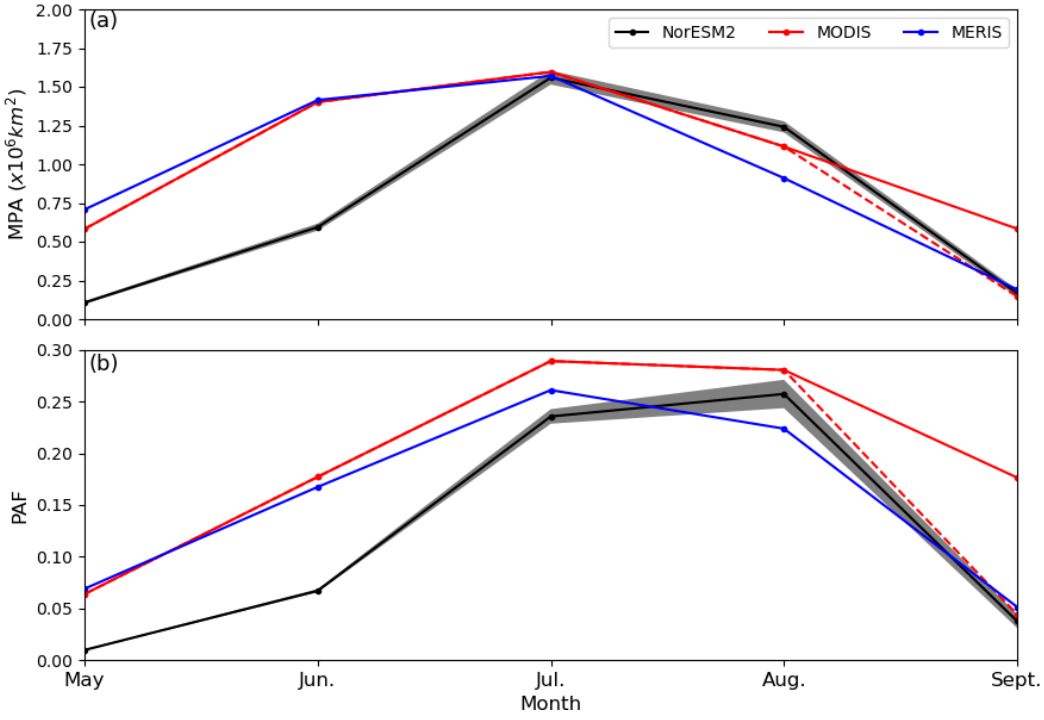

Figure 4. Seasonal cycle of MPA (a) and PAF (b) in NorESM2, MODIS and MERIS during the period of 2002-2011. The gray area is the ensemble spread of MPA and PAF in NorESM2 for the 3 ensemble runs. The red solid lines are for MODIS-High and the red dashed lines are for MODIS-Low.

40% in NorESM2 (Fig. 3m), 50% in MODIS (Fig. 3c) and MERIS (Fig. 3h) over the Arctic Ocean. Between Greenland and the North Pole, the RMPF was similarly low as MPF, 10-20% in NorESM2, 15-25% in MODIS and 20-30% in MERIS, and at the same time, the region with RMPF of 25-30% was much smaller in NorESM2 than in MODIS and MERIS. In the Canadian bays/straits, the RMPF was higher in NorESM2 than in MODIS and MERIS. These features were also found in August. The NorESM RMPF was again found in a much larger area than that in MODIS and MERIS in same regions as MPF.

On the whole, the magnitudes of MPF and RMPF in NorESM2 were lower than those in MODIS and MERIS in May, June and September and more comparable in July and August. This indicates that the MPs in NorESM2 formed later and developed faster than in the observations.

3.2 Seasonal evolutions of MPs area on all sea ice types

3.2.1 MPA and PAF in the Pan-Arctic

Figure 4 shows the seasonal evolutions of MPs area in the Pan-Arctic for MPA (the total area covered by ponds; Fig. 4a) and PAF (the pond area relative to sea ice area; Fig. 4b). Consistent with the spatial distributions of the MPF with time (Fig.

https://doi.org/10.5194/egusphere-2026-1525
Preprint. Discussion started: 30 April 2026

Table 1. The multi-year seasonal mean (May - September) MPA and PAF in NorESM2, MODIS and MERIS in the Pan-Arctic, and in the Pacific, Atlantic, Laptev and Canadian sectors.

	MPA(x10^6 km^2)					PAF				
	Pan-Arctic	Pacific	Atlantic	Laptev	Canadian	Pan-Arctic	Pacific	Atlantic	Laptev	Canadian
NorESM2	0.73	0.28	0.08	0.13	0.24	0.12	0.12	0.10	0.12	0.14
MODIS-High	1.06	0.45	0.14	0.23	0.24					
MODIS-Low	0.97	0.42	0.13	0.20	0.22	0.17	0.18	0.16	0.16	0.16
MERIS	0.96	0.43	0.11	0.21	0.21	0.15	0.17	0.14	0.15	0.14

2), the seasonal evolution of MPA showed that MPA increased from May to July and decreased afterward in NorESM2 and in the two observations (Fig. 4a). Similarly seasonal MPs evolution was also reported by previous studies (Perovich et al., 2002b; Webster et al., 2015; Peng et al., 2022; Webster et al., 2022; Xiong and Ren, 2023), although the seasonal evolution may vary in different regions and years (Niehaus et al., 2025). The MPA in MERIS was slightly higher (0.13x10^6 km^2) than that in MODIS in May, and became closer to those in MODIS (0.01-0.02x10^6 km^2) in June and July. Afterward, it was lower (0.20x10^6 km^2) than that in MODIS in August, and much lower (0.39x10^6 km^2) than that in MODIS-High and close to that in MODIS-Low (difference: 0.05x10^6 km^2) in September. Thus, the seasonal mean of MPA was 0.96x10^6 km^2, 1.06x10^6 km^2 and 0.97x10^6 km^2 in MERIS, MODIS-High and MODIS-Low (Table1), indicating the better agreement of MPA in MERIS with MODIS-Low than with MODIS-High.

Compared to MERIS and MODIS, the NorESM2 MPA was obviously much lower, being 0.60x10^6 km^2 and 0.48x10^6 km^2 in May and 0.82x10^6 km^2 and 0.81x10^6 km^2 in June, respectively. From June onward, it agreed well with those in MODIS and MERIS in July (difference: 0.01-0.04x10^6 km^2), but was 0.33x10^6 km^2 larger than MERIS and 0.13x10^6 km^2 larger than MODIS in August (Fig. 5a). In September, the MPA in NorESM2 was notably lower (0.42x10^6 km^2) than that in MODIS-High while slightly lower (0.02x10^6 km^2) than that in MODIS-Low. The seasonal mean of MPA was 0.73x10^6 km^2 in NorESM2, which was about 31%, 25% and 24% lower than those in MODIS-High, MODIS-Low and MERIS, respectively, mainly due to the significant underestimation in May and June.

The seasonal evolutions of PAF in the observations showed a similar seasonal cycle to the MPA (Fig. 4b vs. 4a), increasing from May to July and decreasing afterward. The PAF consistently reached maximum in July in the observations of MODIS and MERIS, although the PAF in MODIS had no big difference (<0.01) between July and August. The PAF in MERIS was close to that in MODIS in May and June, but became lower in July and August. In September, it was still lower than MODIS-High but closer to MOIDS-Low. As a result, the seasonal mean in MERIS (0.15) was slightly lower than that in MODIS-Low (0.17), and much lower than that in MODIS-High (0.20) (see Table 1).

The PAF in NorESM2 reached the maximum in August, one month later than in the observations. It was again clearly greatly underestimated in May and June. In July, it was still underestimated but much closer to the observations. In August, it was between MODIS and MERIS. In September, it was close to MERIS and MODIS-Low, but much lower than MODIS-High. On

https://doi.org/10.5194/egusphere-2026-1525
Preprint. Discussion started: 30 April 2026

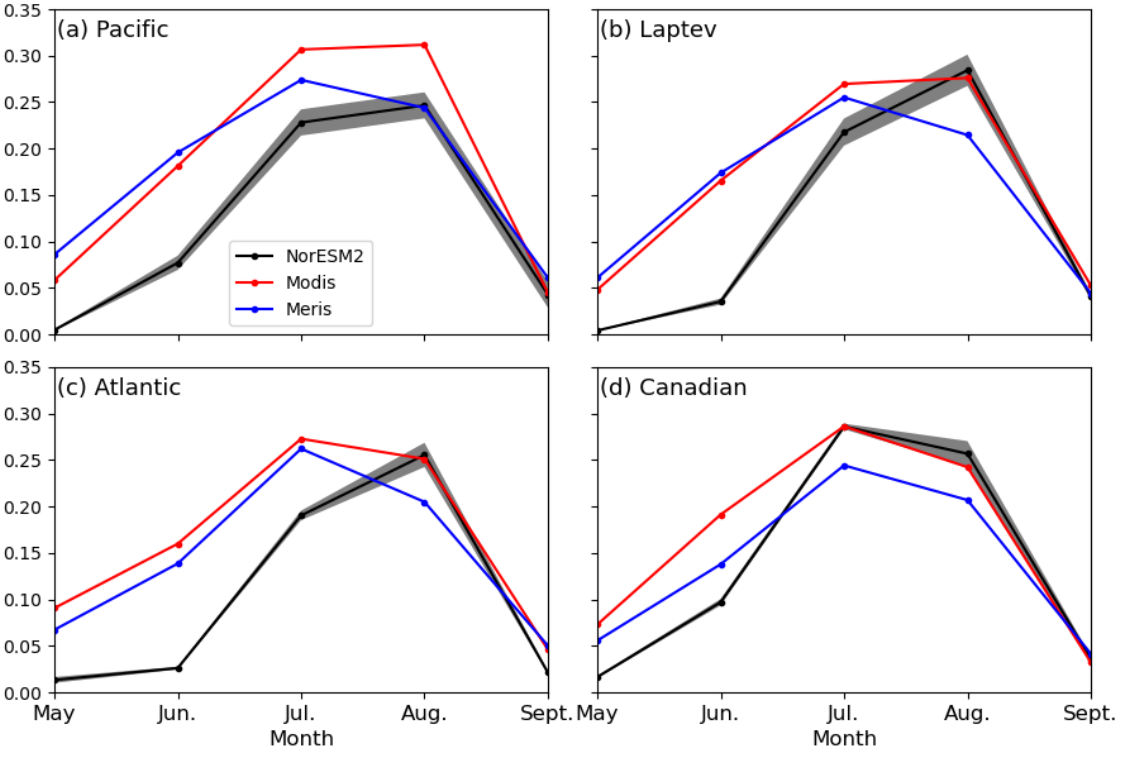

Figure 5. Seasonal cycles of PAF in the subregions of (a) Pacific, (b) Laptev, (c) Atlantic, and (d) Canadian in NorESM2, MODIS and MERIS. MODIS-Low was used here.

the whole, the seasonal mean of PAF in NorESM2 was 0.12, which was underestimated by 40%, 29% and 20% compared to MODIS-High, MODIS-Low and MERIS, respectively, mainly due to the significant underestimation in May and June.

As shown above, the MPA and PAF in MERIS in September was closer to those in MODIS-Low but much lower than those in MODIS-High. This implies that the assumption of zero MPF after mid-September in MODIS-Low might be reasonable since most of MPs refrozen after mid-September and there were only small patches of MPs in the southern latitudes. Therefore, we discard MODIS-High and only make use of MODIS-Low below.

Sea ice in NorESM2 usually covers a more larger area than observations as mentioned above (see Fig. 2-3) due to the larger sea ice area in NorESM2. This larger area can to some degree offset the less MPs in NorESM2 and produce a larger MPA. To lessen the effect of the total sea ice area, we focus on PAF in the following.

3.2.2 PAF in the sub-regions - Pacific, Atlantic, Laptev and Canadian

The seasonal cycles of the PAF in all the sub-regions on all sea ice types were shown in Fig. 5. The observed PAFs reached their peaks in July in all the four sub-regions although the PAF in MODIS had no big differences in July and August in the Pacific and Laptev sectors (Fig. 5a & 5b). By contrast, the simulated PAF in NorESM2 reached a peak in July only in the

https://doi.org/10.5194/egusphere-2026-1525
Preprint. Discussion started: 30 April 2026

Canadian sector but in August in the other three sub-regions, which was one month later compared to the observations in the same sub-regions.

The observed PAF in MODIS and MERIS had more or less differences from May to September in the four sub-regions. In the Pacific, Laptev and Atlantic sectors, the PAF differences between MODIS and MERIS were usually small (≤ 0.03) in May, June and September whether the PAF in MODIS was larger than that in MERIS or the opposite, and became larger in July and August (Fig 5a-c). The much larger PAF in MODIS than in MERIS was also found in the months of July and August in the Canadian region, as well as in June in the same sub-region (Fig. 5d). In May and September, the PAF differences between MODIS and MERIS in the Canadian sector were also small as already seen in the other three sub-regions. Overall, the seasonal mean of PAF in MODIS was 0.01-0.02 larger than that in MERIS in the four sub-regions (Table 1). In spite of the differences, the seasonal mean of PAF was the largest in the Pacific region, but more comparable in the other three sub-regions.

Figure 5 also compares the PAF in NorESM2 with those in MODIS and MERIS for the four sub-regions. The NorESM2 PAF was considerably lower than the observations in the four sub-regions in May and June, and noticeably lower in the Pacific, Laptev and Atlantic regions in July (Fig. 5a-c). However, it turned to be higher than the observation in MERIS while agreed with the observation in MODIS in the Canadian region in the same month (Fig. 5d). In August, the PAF in NorESM2 agreed well with the observations, although it was with MERIS in the Pacific region (Fig. 5a) and with MODIS in the rest three sub-regions (Fig. 5b-d). In addition, the disagreement was also apparent in August, for example, the larger PAF in NorESM2 than in MERIS in the Laptev, Atlantic and Canadian regions, or the smaller PAF in NorESM2 than in MODIS in the Pacific region. In September, the PAF in NorESM2 was generally consistent with the observations in MODIS and MERIS in the four sub-regions.

The seasonal mean of PAF in NorESM2 was 0.12, 0.10, 0.12, 0.14 in the Pacific, Atlantic, Laptev and Canadian regions, respectively. These values were notably lower than those in MODIS and MERIS in the former three regions, as well as that in MODIS in the Canadian region, but equal to that in MERIS in the Canadian region (Table 1). Thus, the bias of PAF in NorESM2 was -0.06, -0.06, -0.04 and -0.02 relative to MODIS, and -0.05, -0.04, -0.04 and 0 relative to (MERIS) in the Pacific, Atlantic, Laptev and Canadian regions. The RE of PAF in NorESM2 was -33%, -38%, -25%, and -12% relative to MODIS, and -29%, -29%, -20% and 0% relative to MERIS in the Pacific, Atlantic, Laptev and Canadian regions, respectively. The RMSE of the seasonal mean of PAF in NorESM2 varied from 0.05 to 0.08 relative to the observations, with the lowest RMSE in the Canadian region, and the highest RMSE in the Atlantic region for MODIS but in the Laptev region for MERIS.

The spread of PAF of the 3 NorESM2 ensembles varied in the four sub-regions and from May to September (Fig. 5). The differences are larger in the Pacific sectors, and relatively small in the other three regions, and smaller in May and June and larger in July and August.

https://doi.org/10.5194/egusphere-2026-1525
Preprint. Discussion started: 30 April 2026

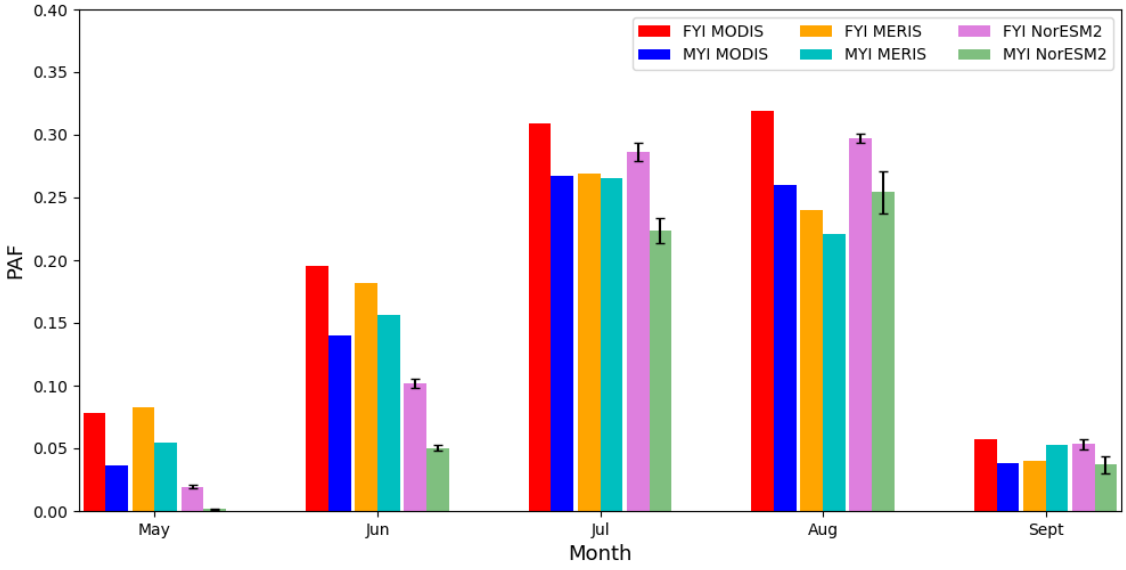

Figure 6. PAF on FYI and on MYI in NorESM2, MODIS and MERIS from May to September during the period of 2002-2011 in the Pan-Arctic. The error bars show the standard deviations of the NorESM2 ensembles around the mean.

3.3 PAF on different ice types: FYI and MYI

3.3.1 Pan-Arctic

The seasonality of PAF was obvious both on FYI and MYI in the observations and in NorESM2 (Fig. 6). However, the occurrence time of the PAF maximum was varying on different ice types in the two observations and NorESM2. The observed PAFs in MERIS clearly reached their maximum in July both on FYI and on MYI. In contrast, the PAF in MODIS reached its maximum on MYI in the same month as in MERIS while in August on FYI, one month later than in MERIS. In addition, the largest PAF in MODIS was only slightly larger than its previous month on FYI and its next month on MYI. Compared to the observations, the simulated PAF in NorESM2 reached the maximum in August regardless of the ice types.

The PAF on FYI was consistently higher than that on MYI from May to September whether in the observations or in NorESM2, except MERIS in September (Fig. 6). The higher fraction of MPs on FYI than MYI was consistent with previous studies, e.g., Perovich and Polashenski (2012), Polashenski et al. (2012) and Li et al. (2020), indicating the fast development of MPs on FYI than on MYI. However, pond drainage took place within a few days (Perovich and Polashenski, 2012), resulting in a dramatic/slight decrease of MPF on sea ice. This phenomenon could not be identified by the monthly mean data here.

The differences in the observed PAF between MODIS and MERIS varied over time and across ice types (Fig. 6). In May, June and September, The PAF differences in MODIS and MERIS were generally small (<0.02), regardless of whether the PAF in MODIS was higher than in MERIS on FYI or lower on MYI. In July, the differences remained small (0.002) on MYI but increased significantly on FYI (0.04). Similarly, in August, the differences grew to 0.04 on MYI and 0.08 on FYI. Overall, the

https://doi.org/10.5194/egusphere-2026-1525
Preprint. Discussion started: 30 April 2026

Table 2. The seasonal mean (May - September) PAF in NorESM2, MODIS and MERIS in the Pan-Arctic, and in the Pacific, Atlantic, and Laptev sectors on FYI and MYI during 2002-2011.

	Pan-Arctic	Pacific	Atlantic	Laptev
FYI NorESM2	0.15	0.13	0.11	0.14
FYI MODIS	0.19	0.20	0.20	0.17
FYI MERIS	0.16	0.18	0.15	0.16
MYI NorESM2	0.11	0.12	0.10	0.10
MYI MODIS	0.15	0.16	0.15	0.13
MYI MERIS	0.15	0.16	0.14	0.12

seasonal mean PAF was 0.19 for MODIS and 0.16 for MERIS on FYI, while both observations recorded a mean PAF of 0.15 on MYI. This highlights a larger seasonal difference (0.13) between MODIS and MERIS on FYI compared to on MYI.

Compared to the observations, the simulated PAF in NorESM2 was noticeably lower in May and June but became more aligned with the observations in later months, both on FYI and MYI. Specifically, in July, the simulated PAF remained lower than both MODIS and MERIS on MYI, while it fell between the two observations in July and August on FYI and in August on MYI. The biases betwen NorESM2 and MODIS/MERIs were -0.03/0.02 in July and -0.02/0.06 in August on FYI. On MYI, the biases were -0.04/-0.04 in July and -0.01/0.03 in August. Overall, the seasonal mean of PAF in NorESM2 was 0.15 on FYI and 0.11 on MYI, which was 0.04 lower than MODIS on both FYI and MYI, and 0.01 and 0.04 lower than those in MERIS on FYI and on MYI, respectively. Correspondingly, the RE of PAF in NorESM2 was -21% and -6% on FYI, and -27% on MYI compared to MODIS and MERIS, respectively, and the RMSE of PAF in NorESM2 was 0.09/0.03 on FYI and 0.08/0.08 on MYI relative to MODIS/MERIS.

In the following analysis, we exclude the Canadian region and focus on the Pacific, Atlantic and Laptev regions. The Canadian region contains numerous narrow straits within the Canadian Archipelago, which pose challenges for satellite tracking by NSIDC. Due to the inability of NSIDC's tracking methodology to navigate these narrow straits, the computation of sea ice age in NSIDC in these areas is limited (personal communication). As a result, sea ice in the NSIDC is often either identified as no ice or classified as FYI in these regions (Fig. 8a & 8b), although it seems there are not only FYI but also MYI in these areas (Fig. 8c & 8d).

3.3.2 Sub-regions: Pacific, Laptev and Atlantic

The seasonal cycles of PAF were pronounced on FYI and MYI in the observations and NorESM2 across the Pacific, Laptev and Atlantic sub-regions (Fig. 7), similar to the patterns observed in the pan-Arctic (Fig. 6). However, the occurrence time of the maximum PAF varied across the three sub-regions and ice types, even between the two observations of MODIS and MERIS. In MERIS, the PAF consistently culminated in July across the three regions, regardless of ice type (Fig. 7). In contrast, the maximum PAF in MODIS occurred in July in the Atlantic region for both FYI and MYI (Fig. 7c), aligning with the peak timing in MERIS. However, in the Pacific and Laptev regions, the largest PAF in MODIS was observed in August for both

https://doi.org/10.5194/egusphere-2026-1525
Preprint. Discussion started: 30 April 2026

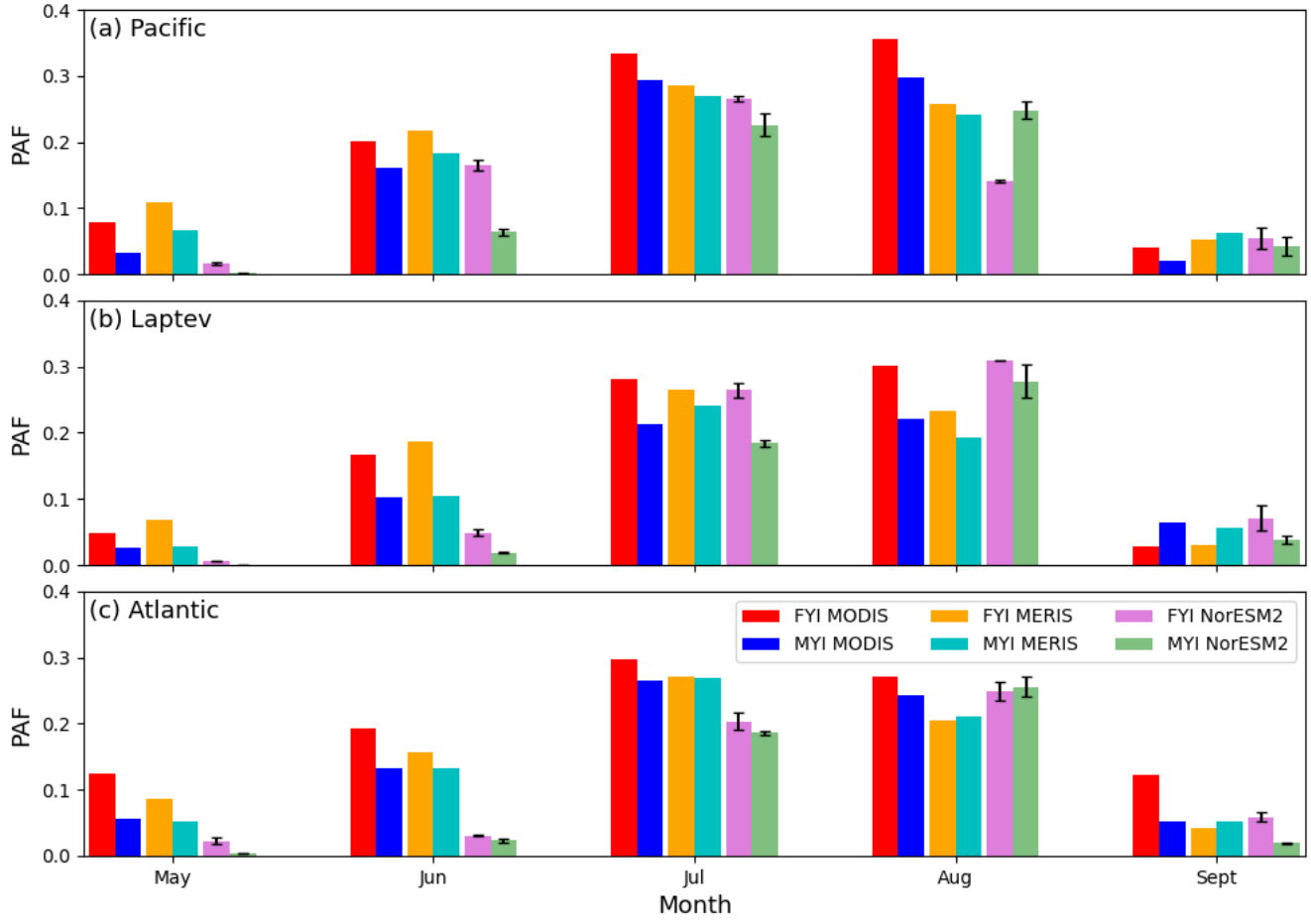

Figure 7. same as Fig. 6, but in the sub-regions of (a) the Pacific, (b) the Laptev, and (c) the Atlantic.

FYI and MYI (Fig. 7a & 7b), one month later than in the Atlantic region and one month later than the peaks in MERIS for the same regions and ice types. Similarly, the simulated maximum PAF in NorESM2 displayed regional and ice-type dependent variation. In the Laptev and Atlantic regions, the peak PAF occurred in the same month - August - for both FYI and MYI (Fig. 7b & 7c). However, in the Pacific region, the peak occurred in different months depending on the ice type: July on FYI and August on MYI (Fig. 7a).

The PAFs in MODIS and MERIS were persistently higher on FYI than on MYI from May to August in the Pacific region (Fig. 7a) and the Laptev region (Fig. 7b). In September, the PAF on FYI remained higher than on MYI in MODIS for the Pacific region, but dropped below MYI in MERIS for the same region. In contrast, in the Laptev regon, the PAF on FYI became lower than on MYI in both MODIS and MERIS in September (Fig. 7b). In the Atlantic region, the PAF on FYI was greater than on MYI in MODIS throughout the entire period from May to September. However, in MERIS, the PAF on FYI exceeded that on MYI only until July, afterward it became smaller (Fig. 7c). These results align with previous studies (e.g., Webster et al. 2015;

https://doi.org/10.5194/egusphere-2026-1525
Preprint. Discussion started: 30 April 2026

Lee et al. 2024; Niehaus et al. 2025), which reported a higher fraction of MPs on MYI compared to FYI due to earlier MPs formation on MYI. Overall, the seasonal mean of PAF on FYI was higher than on MYI by 0.04/0.02, 0.05/0.01 and 0.04/0.04 in MODIS/MERIS for the Pacific, Atlantic and Laptev regions, respectively (see Table 2).

In NorESM2, the PAF on FYI was consistently higher than on MYI in the Laptev (Fig. 7b) and Atlantic (Fig. 7c) regions. The seasonal mean difference of PAFs between FYI and MYI was 0.01 in the Atlantic region and 0.04 in the Laptev region. In the Pacific region, the PAF on FYI was larger than on MYI until July, after which the trend reversed, with MYI showing higher PAF values. The seasonal mean difference of PAF between FYI and MYI was 0.01, the same as in the Atlantic region (Table 2). However, this small seasonal mean difference in the Atlantic region resulted from the consistently small differences throughout the season (Fig. 7c), whereas in the Pacific region, it was due to the offsetting of positive difference earlier in the season and negative differences later on (Fig. 7a).

The differences in PAF between MODIS and MERIS were generally small (<0.04) in May, June and July in the three sub-regions on both FYI and on MYI, except on FYI in the Pacific region. In August, the differences remained small on MYI in the Laptev and Atlantic regions, but became larger on MYI in the Pacific region and on FYI in all the three sub-regions, particularly on FYI in the Pacific sector (up to 0.1). In September, the differences were again generally small, except on FYI in the Atlantic region. Overall, the seasonal mean PAF in MODIS was larger than in MERIS across all the three sub-regions, regardless ice type. The largest difference was 0.05 on FYI in the Atlantic region, while the smallest difference (0) was observed on MYI in the Pacific region.

Compared to the observations, the PAF in NorESM2 was clearly underestimated on both FYI and MYI during May and June in all the three sub-regions. In July, underestimation persisted, e.g., on FYI in the Pacific region (Fig. 7a), on MYI in the Laptev region (Fig. 7b), and on both FYI and MYI in the Atlantic region (Fig. 7c). However, cases of overestimation also emerged, such as on MYI in the Pacific region (Fig. 7a). In August, the PAF in NorESM2 was clearly underestimated on FYI in the Pacific region (Fig. 7a), while it was notably overestimated on MYI in both the Pacific and Laptev regions compared to the observations from MODIS and MERIS. In addition to these consistent patterns of overestimation and underestimation, there were instances of good agreements with one of the two observations. For example, NorESM2 aligned well with MODIS on FYI in the Laptev and Atlantic regions and on MYI in the Atlantic region (Fig. 7b & 7c) in this month. In September, overestimation, underestimation and agreements were all evident, but the magnitude of the differences was generally small (not over 0.04). Overall, the seasonal mean bias of PAF between NorESM2 and the observations was -0.07(-0.05), -0.09(-0.04) and -0.03(-0.02) on FYI, and -0.04(-0.04), -0.05(-0.04), and -0.03(-0.02) on MYI relative to MODIS/MERIS in the Pacific, Atlantic and Laptev regions, respectively. The corresponding RE was 35% (27%), 45% (27%) and 18% (12%) on FYI, and 25% (25%), 33% (29%) and 23% (17%) on MYI compared to MODIS (MERIS) in the Pacific, Atlantic and Laptev regions, respectively. The RMSE was 0.11(0.07), 0.10(0.07) and 0.06 (0.08) on FYI, and 0.06 (0.06), 0.07 (0.07) and 0.05 (0.06) on MYI in the Pacific, Atlantic and Laptev regions, respectively.

https://doi.org/10.5194/egusphere-2026-1525
Preprint. Discussion started: 30 April 2026

4 Discussion

4.1 Uncertainty of PAF in NorESM2

The uncertainties of PAF in NorESM2 are represented by the ensemble spread as shown in Fig. 5-8. This spread was calculated from the three ensemble members of NorESM2 (see section 2.1.1) and is expressed as the standard deviation (STD) relative to the ensemble mean. The STD of PAF in NorESM2 varied across months, sub-regions and ice types. It was negligible (<=0.002) in May and June, but increased in the following months (Fig. 4b). In July, the larger STD was observed in the Pacific and Laptev regions, while in August, the larger STD increased across all the sub-regions (Fig. 5). Obviously, the larger STD in August was primarily attributed to the large STD on MYI (Fig. 6) in all the three sub-region of the Pacific, Laptev and Atlantic (Fig. 7). In contrast, the larger STD in July was due to larger STD on both FYI and on MYI (Fig. 6), particularly on MYI in the Pacific region and on FYI in the Laptev and Atlantic regions (Fig. 7). The seasonal mean of STD on MYI was largest in the Pacific region, while the seasonal mean of STD on FYI showed no significant differences among the Pacific, Laptev and Atlantic sub-regions. The largest STD of PAF was 0.01, which accounted for 5% of the ensemble mean PAF. These results confirmed that the descriptions of PAF in section 3.2-3.3 are robust. Finally, the consistently small STD in May and June indicates that MPs were systematically underestimated in NorESM2 during these months.

4.2 Sea ice age

Figure 8 illustrates the distribution of FYI and MYI in the NSIDC observations and NorESM2 simulations for July and August. Overall, There was more MYI in NorESM2 than in NSIDC (Fig. 8a, c vs. Fig. 8b, d), such as, in the Greenland Sea. In addition, there was notably no sea ice in the straits/bays in the Canadian Archipelago, nor any MYI in the Nares Strait or west of Greenland in NSIDC. In contrast, there was both FYI and MYI in these regions in NorESM2. This discrepancy arises due to the limitations of NSIDC's tracking methodology, which is unable to classify ice in narrow regions (personal communication), as mentioned earlier. Both NorESM2 and NSIDC identified MYI north of Greenland and north of the Canadian Archipelago. However, NorESM2 simulated more MYI than NSIDC in sub-regions of the Pacific, Laptev and Atlantic, with the Pacific region showing the largest difference. Corresponding to the higher amount of MYI in the Pacific region, NorESM2 simulated less FYI in this region. This contributed to a higher PAF on MYI and a lower PAF on FYI in July and August in the Pacific region (Fig. 7a). The increased PAF on MYI in NorESM2 was offset by the decreased PAF on FYI during July and August (Fig. 7a). As a result, the total PAF in NorESM2 was more comparable to the observations in MODIS and MERIS during these two months in the Pacific region (Fig. 5a).

4.3 Products of MODIS and MERIS

The MPs products from MODIS and MERIS have been comprehensively compared in the Pan-Arctic, within different sub-regions, and over various ice types from May to September during 2002-2011 (Figs. 2-7). For MODIS-low, We assumed zero MPF after mid-September, and the general agreements between MODIS-Low and MERIS in September supports the validity

https://doi.org/10.5194/egusphere-2026-1525
Preprint. Discussion started: 30 April 2026

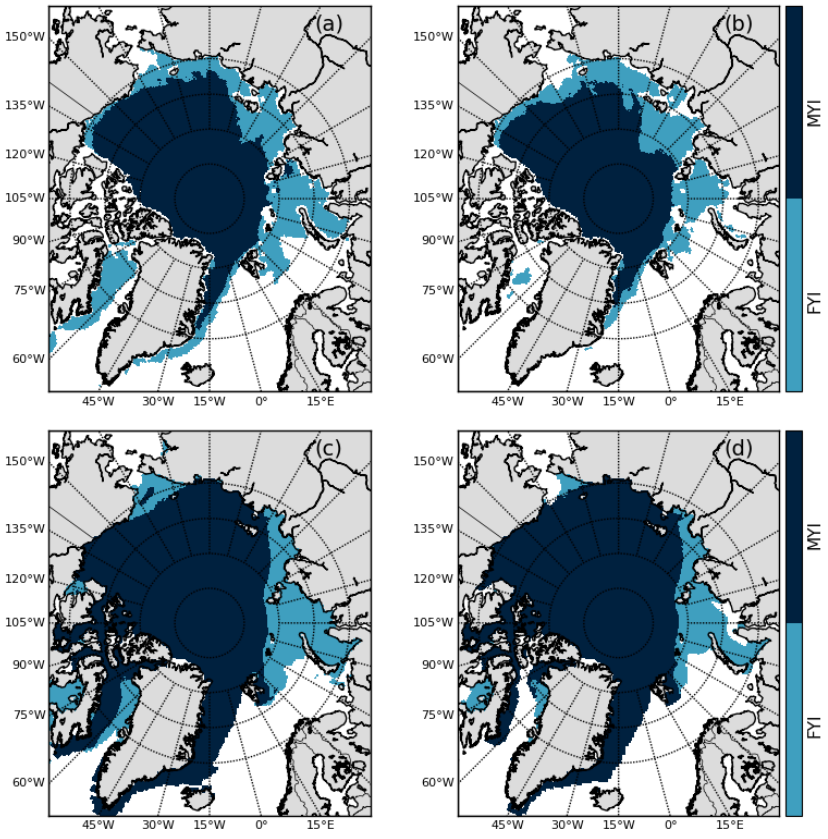

Figure 8. Sea ice age in NSIDC (a, b) and in NorESM2 (c, d) in July (a, c) and in August (b, d)

of this assumption. Additionally, MODIS and MERIS showed similar spatial distributions (Figs. 2-3) and comparable seasonal evolutions (Figs. 4-7). The differences between the two MP products were small in May, June and September, and became more pronounced in July and August when MPs were more abundant. This indicates strong agreements between MODIS and MERIS during the early melt season and the refreezing period, while large discrepancies occur during the peak melt season. These differences can be attributed to the limitations of optical sensors, their coarse spatial resolutions, and the retrieving algorithms. During the melt season, the Arctic surface transforms into a complex mixture of wet snow, leads and cracks between ice floes, open waters, MPs and bare ice. Optical satellites like MODIS and MERIS, with their coarse resolution, has challenges in distinguishing between leads, small areas of open water, and MPs. This increases the likelihood of misidentifying leads or cracks as MPs, especially during the advanced melt season. While higher-resolution satellite offer improved discrimination of leads and cracks, there remains potential for misclassification, as leads and cracks can still be mistaken for MPs rather than open water (Lee et al., 2024). Furthermore, the retrieval algorithms for MP products take into account factors, such as atmospheric correction and the bidirectional reflectance properties of MPs, snow and ice surfaces (Rösel et al., 2012; Istomina

https://doi.org/10.5194/egusphere-2026-1525
Preprint. Discussion started: 30 April 2026

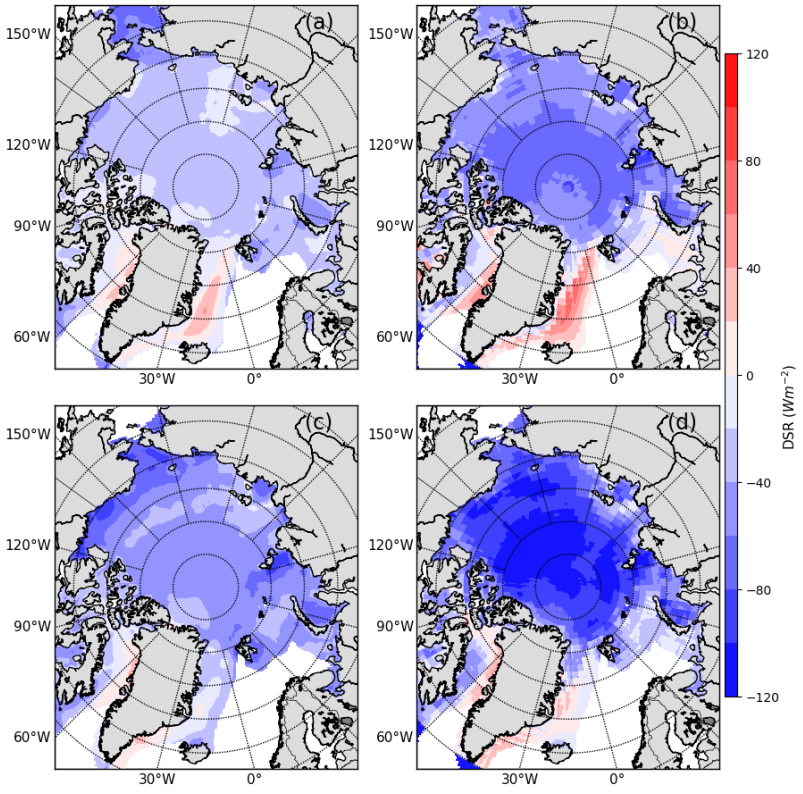

Figure 9. Differences of DSR between NorESM2 and ERA5, and between NorESM2 and CERES in May (a, c) and June (b, d)

et al., 2025). However, biases in the atmospheric correction and assumptions regarding bidirectional reflectance can also lead to unrealistic results during melt season (Zege et al., 2015).

4.4 Low MPs in May and June and surface downward solar radiation (DSR)

As already seen, the MPs in NorESM2 were significantly underestimated in May and June compared to the observations from MODIS and MERIS, both on FYI and MYI in the pan-Arctic and the sub-regions. This underestimation could be attributed to either an overestimation of MPs in MODIS and MERIS observations or an underestimation in NorESM2. The overestimation of MPs in MODIS and MERIS may result from the following factors: (i) Clouds, which influence the surface reflectance, possibly leading to higher MPF values in the observations (Ding et al., 2020). For instances, MPF was found to be reduced by 0.5-3.2% during 2003-2011 when only data under clear-sky conditions were used, compared to data used under both clear and cloudy conditions (Ding et al., 2020); (ii) open water and leads, their presences can significantly alter the surface albedo, and may be misidentified as MPs due to the coarse spatial resolution of the sensors (Lee et al., 2024). On the other hand, the underestimation of MPs in NorESM2 may be related to the low DSR in NorESM2. AS shown in Figure 9, the DSR was consistently underestimated in May and June over most of the Arctic sea ice in NorESM2 compared to ERA5 (Fig. 9a & c)

https://doi.org/10.5194/egusphere-2026-1525
Preprint. Discussion started: 30 April 2026

and SYN1deg (Fig. 9b & d), with the underestimation being particularly pronounced compared to SYN1deg. In May, the DSR underestimation was relatively small, ranging from 20-40 Wm^{-2} compared to ERA5, and typically 40-80 Wm^{-2} compared to SYN1deg. However, the underestimation was relatively large in June, reaching 20-60 Wm^{-2} relative to ERA5, and 80-120 Wm^{-2} relative to SYN1deg. The underestimation of DSR might be linked to an overestimation of cloud cover. Over the Arctic sea ice, the total cloud fraction was usually found to be 0.8-1.0 in May and 0.8-0.9 in June in ERA5, while, it was slightly lower, 0.6-1.0 in May, and 0.6-0.9 in June in CERES. This suggests that NorESM2 could overestimate total cloud fraction by up to 0.4, contributing to the reduced DSR and consequently, the lower simulated MPs.

4.5 The impact of DSR in ICEPACK

In this section, ICEPACK, the column version of CICE, was used to study the impact of DSR on the early formation of MPs. The experiments were conducted using data from an Ice Mass Balance buoy (IMB; Richter-Menge et al., 2006), specially IMB2004B (Perovich et al., 2022; http://imb-crrel-dartmouth.org). IMB2004B was deployed on a MYI floe with an ice thickness of 2.2 m and a snow depth of 0.26 m on 24 April 2004 near the North Pole (85.9^oN, 94.0^oE). After deployment, the ice floe with IMB2004B drifted westward, reaching 84.9^oN and 71.4^oE by the end of August (Fig. 1). According to the observations from IMB2004B, the snow depth remained stable at approximately 0.26 m until 4 May. It then increased slightly to over 0.3 m during 4-8 May, before stabilizing around 0.28 m until 4 June. From 4 June onward, the snow depth increased to 0.33 m on 4 June and remained at this depth until 12 June. After 12 June, snow started to melt, with the snow disappearing completely by 18 June (Fig. 10a). Melt at the ice surface commenced on 18 July.

The ICEPACK simulation was performed using the initial snow and ice conditions from 4 May, with the atmospheric forcing from ERA5. Overall, ICEPACK normally captured the evolution of snow and ice observed by IMB2004B. However, it fails to accurately reproduce two episodes of snow depth increase (4-8 May and 4-12 June). During the first episode (4-8 May), the lack of precipitation in ERA5 resulted in no snow depth increase in the simulation. The observed snow depth increase during this period can likely be attributed to snow drifting against the IMB structure, as evidenced by an increase in wind speed. This phenomenon of of snow accumulation against IMB structure has been documented by Wang et al. (2019). In the second episode (4-12 June), while the simulation showed a slight snow depth increase, it was notably lower than the observed increase. This discrepancy can be attributed to insufficient precipitation in ERA5 during this period. The snow melt onset was well simulated by ICEPACK. However, the snow melted faster in the simulation, leading to the disappearance of snow earlier than observed (Fig. 10a). Consequently, ice melt also began earlier in the simulation. Before the onset of snowmelt, ice melting at the bottom of the ice floe had already started in late May (Fig. 10b). After the snow had completely melted, surface ice melt began. As observed, there was more melting at the ice surface than at the ice bottom. A abrupt increase in ice thickness increase of approximately 0.2 m at the ice bottom was recorded by IMB2004B in early July, believed to caused by the formation of a false bottom (Untersteiner and Badgley, 1958; Eicken et al., 2002). Such false bottoms have been observed in IMB deployments, such as in Rijpfjorden, Svabard (Wang et al., 2013). However, Icepack lacks the capacity to simulate the formation of false bottoms, which led to a significant divergence between the simulated ice thickness and observed ice thickness from early July. MPs start to form in late June, quickly reaching their peak before steadily decrease thereafter.

https://doi.org/10.5194/egusphere-2026-1525
Preprint. Discussion started: 30 April 2026

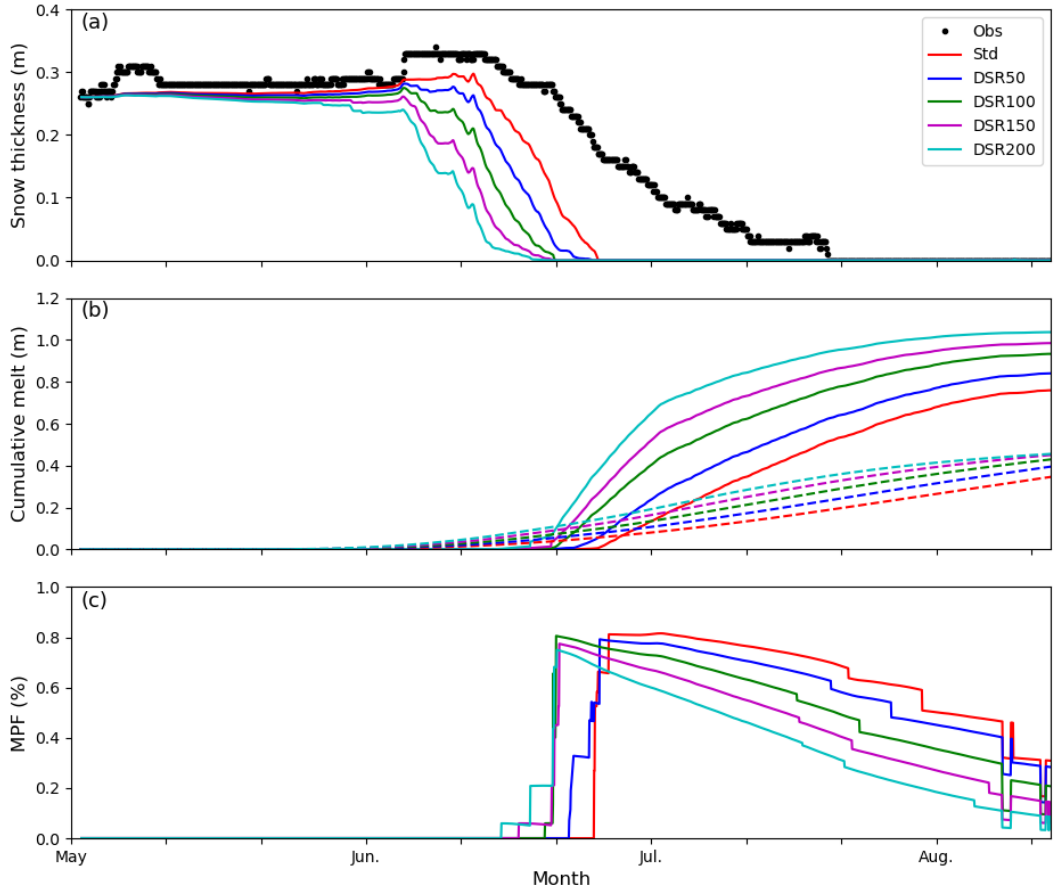

Figure 10. (a) Observed and simulated snow thickness, and (b) cumulative melt at the ice surface (solid lines) and bottom (dashed lines), and (c) MPF in the simulations with DSR from ERA5 (std.), DSR+50 Wm^{-2} (DSR50), DSR+100 Wm^{-2} (DSR100), DSR+150 Wm^{-2} (DSR150), and DSR+200 Wm^{-2} (DSR200).

The influences of DSR on MPs are investigated by increasing the DSR in ERA5 by 50 Wm^{-2} (SR50), 100 Wm^{-2} (SR100), 150 Wm^{-2} (SR150) and 200 Wm^{-2} (SR200) during May and June (Fig. 10). The results show that increasing the DSR had no big influences on snow depth for most of May (Fig. 10a). However, starting in early June, the increased DSR led to a reduction in snow depth and enhanced ice melting, particularly at the ice surface, which experienced more melting than the ice bottom. As DSR increased, snow began melting earlier and disappeared sooner, which in turn triggered earlier MPs formation (Fig. 10c). This is because snowmelt reduces surface albedo, thereby amplifying the effect of DSR on melting the snow-ice surface (Persson, 2012). Our experiments demonstrate that increasing DSR results in earlier MPs formation, suggesting that the underestimated DSR in NorESM2 contributed to its underestimation of MPs formation. However, the cause of early MP formation observed in May remains unclear.

https://doi.org/10.5194/egusphere-2026-1525
Preprint. Discussion started: 30 April 2026

5 Conclusions

NorESM2, the second generation of the coupled earth system developed by the Norwegian Climate Center, serves as a valuable tool for researchers to study past, present and future climate. However, the performance of NorESM2 in simulating MPs has not yet been thoroughly evaluated, despite the crucial role of MPs play in the Arctic climate system and ecosystem. In this study, we assessed the representation of MPs in NorESM2 using monthly data from MODIS and MERIS. The evaluation focus on four variables: MPF, RMPF, MPA and PAF, with particular emphasis on PAF. The analysis was conducted for the pan-Arctic, its sub-regions, and on FYI and MYI from May to September during 2002-2011. To address the lack of data after mid-September in MODIS, a zero MPF assumption was applied, referred to as MODIS-Low.

Despite some differences, MODIS and MERIS demonstrated similar spatial distributions and season evolutions of MPs across all ice types in the pan-Arctic and sub-regions. Both datasets consistently showed a larger fraction of MPs on FYI compared to on MYI in these regions. While MERIS consistently recorded the maximum fraction of MPs in July, MODIS sometimes showed the peak in August, depending on the sub-regions or ice types. The differences in PAF between MODIS and MERIS varied with season, sub-regions, and ice types. They were relatively small in May, June and September, but became more pronounced in July and August. The greater consistency in May, June and September suggests that both products provide a better representation of MPs in the early melt season and the refreezing season. In contrast, the large discrepancies in July and August are likely due to the challenges of retrieving MPF using coarse-resolution optical sensors. This limitation makes it difficult to determine which product performs better for observing MPs during the peak melt season. To improve the quality of MP products, higher-resolution or non-optical sensors may offer a more reliable alternative, as suggested by (Buckley et al., 2023).

NorESM2 generally reproduces the spatial distribution and seasonal evolution of MPs, although MPs formation in the model occurs later and develops more rapidly compared to observations. Additionally, the maximum PAF in NorESM2 typically occurs in August, except on FYI in the Pacific region. Consistent with observations, the PAF on FYI is larger than on MYI in the Laptev and Atlantic sub-regions throughout the season, as well as in the Pacific region from May to July. The systematic underestimation of MPs in May and June can be partially attributed to the low DSR in NorESM2, likely due to an overestimation of clouds cover. Additionally, the potential overestimation of MPF in MODIS and MERIS could also contribute to these discrepancies, driven by cloud effects, the coarse spatial resolutions of the sensors, and the misidentification of open water and leads as MPs. The overestimation of PAF on MYI in the Pacific region is likely linked to the higher amount of MYI simulated in this region and possibly due to differences in the definition of sea ice age between NorESM2 and NSIDC.

Using ICEPACK, the column version of CICE, we found that increasing DSR in May and June leads to an earlier MP formation. This finding further reinforces the conclusion that the lower DSR in NorESM2 contributes to the underestimation of MPs during these months. The low albedo of MPs, compared to bare ice and snow, allows more solar radiation to penetrate the sea ice and the upper ocean. Consequently, the absence of MPs in NorESM2 during May and June could lead to higher surface reflectivity and reduced absorption of solar energy, ultimately influencing the evolution of Arctic sea ice, as well as the broader climate system and the ecosystem. Addressing biases in DSR and improving the accuracy of observational retrievals

https://doi.org/10.5194/egusphere-2026-1525
Preprint. Discussion started: 30 April 2026

of MPF are critical steps toward enhancing the performance of the model. Given the vital role of melt ponds, improving their representation in NorESM2 is essential for advancing our understanding of Arctic climate dynamics and the interactions between the cryosphere and the global climate system.

Code and data availability.

All data used in this study are publicly available at the following URL: melt ponds fraction from MODIS at https://www.cen.uni-hamburg.de/en/icdc/data/cryosphere/arctic-meltponds.html, and from MERIS at https://data.seaice.uni-bremen.de/meris/mecosi/, sea ice age from NSIDC at https://daacdata.apps.nsidc.org/pub/DATASETS/nsidc0611_seaice_age_v4/data/, sea ice concentration from AMSR-E at https://data.seaice.uni-bremen.de/amsre/asi_daygrid_swath/n3125/, and ERA5 data at https://cds.climate.copernicus.eu/datasets/reanalysis-era5-single-levels-monthly-means?tab=download.

Author contributions.

CW prepared the data and conducted the core analysis, created the visualization, and drafted the manuscript with feedback and editing from KW and JD. Both KW and JD contributed to data preparation, and provided insightful comments on the manuscript. KW contributed to the data analysis, and all authors contributed to the reviewing, and finalizing the manuscript.

Competing interests.

The contact author has declared that none of the authors has any competing interests.

Acknowledgements. The authors acknowledge colleague Signe Aaboe providing tracking information of sea ice age. The study was supported by the Nordic Council of Ministers through project NOCOS DT (grant no. 102642), the Norwegian Research Council through project 4SICE (grant no. 328886), the Norwegian FRAM Flagship program through project SUDARCO (grant no. 551323), and the EU project ACCESS (grant no. 281010100).

https://doi.org/10.5194/egusphere-2026-1525
Preprint. Discussion started: 30 April 2026

References

Aparício, S.: Review article: Earth observations of melt pond on sea ice, The Cryosphere Discusion [preprint], https://doi.org/10.5194/tc-2023-75, 2023.

Arrigo, K. R., Perovich, D. K., Pickart, R. S., Brown, Z. W., and et al.: Massive phytoplankton blooms under Arctic sea ice, Science, 336(6087), https://doi.org/10.1126/science.1215065, 2012.

Bentsen, M., Bethke, I., Debernard, J. B., Iversen, T., Kirkevåg, A., Seland, , Drange, H., Roelandt, C., Seierstad, I. A., Hoose, C., and Kristjánsson, J. E.: The Norwegian Earth Sys-tem Model, NorESM1-M – Part 1: Description and basic evaluation of the physical climate, Geosci. Model Dev., 6, 687–720, https://doi.org/10.5194/gmd-6-687-2013, 2013.

Bitz, C. M., Holland, M. M., Weaver, A. J., and Eby, M.: Simulating the ice-thickness distribution in a coupled climate model, J. Geophys. Res. Oceans, 106, 2441–2463, 2001.

Bonan, D. B., Schneider, T., Eisenman, I., and Wills, R. C. J.: Constraining the date of a seasonally ice-free Arctic using a simple model, Geophys. Res. Lett., 48(18), e2021GL094309, https://doi.org/10.1029/2021gl094309, 2021.

Briegleb, B. P. and Light, B.: A Delta-Eddington Mutiple Scattering Parameterization for Solar Radiation in the Sea Ice Component of the Community Climate System Model, Tech. Rep. No. NCAR/TN-472+STR, University Corporation for Atmospheric Research, Boulder, Colerado, USA, 10.5065/D6B27S71, 2007.

Buckley, E. M., Farrell, S. L., Herzfeld, U. C., Webster, M. A., Trantow, T., Baney, O. N., Duncan, K. A., Han, H., and Lawson, M.: Observing the evolution of summer melt on multiyear sea ice with ICESAT-2 and Sentinel-2, The Cryosphere, 17, 3695-3719, https://doi.org/10.5149/tc-17-3695-2023, 2023.

Buth, L. G., Krumpen, T., Neckel, N., Webster, M. A., Birnbaum, G., Fuchs, N., Heuser, P., Johannsen, O., and Haas, C.: Characterizing sea ice melt pond fraction and geometry in relation to surface morphology, The Cryosphere, 19(12), 6527-6545, https://doi.org/10.5194/tc-19-6527-2025, 2025.

C3S: Climate Indicators: Sea ice as a climate indicator from the Copernicus Climate Change Service. https://climate.copernicus.eu/climate-indicators/sea-ice, 2022.

Comiso, C., Parkinson, C. L., Gersten, R., and Stock, L.: Accelerated decline in the Arctic sea ice cover, Geophys. Res. Lett., 35, L01703, https://doi.org/10.1029/2007GL031972, 2008.

Danabasoglu, G., Lamarque, J.-F., Bachmeister, J., Bailey, D. A., DuVivier, A. K., Edwards, J., Emmons, L. K., Fasullo, J., Gar-cia, R., Gettelman, A., Hannay, C., Holland, M. M., Large, W. G., Lawrence, D. M., Lenaerts, J. T. M., Lindsay, K., Lipscomb, W. H., Mills, M. J., Neale, R., Oleson, K. W., Otto-Bliesner, B., Phillips, A. S., Sacks, W., Tilmes, S., van Kampenhout, L., Vertenstein, M., Bertini, A., Dennis, J., Deser, C., Fischer, C., Fox-Kember, B., Kay, J. E., Kinnison, D., Kushner, P. J., Long, M. C., Mickelson, S., Moore, J. K., Nienhouse, E., Polvani, L., Rasch, P. J., and Strand, W. G.: The Community Earth System Model version 2 (CESM2), J. Adv. Model. Earth Sy., 12, e2019MS001916, https://doi.org/10.1029/2019MS001916, 2020.

Diamond, R., Sime, L. C., Schroeder, D., and Guarino, M.-V.: The contribution of melt ponds to enhanced Arctic sea-ice melt during the Last Interglacial, The Cryosphere, 15, 5099-5114, https://doi.org/10.5194/tc-15-5099-2021, 2021.

Diamond, R., Schroeder, D., Sime, L. C., Ridley, J., and Feltham, D.: The significance of the melt-pond scheme in a CMIP6 global climate model, J. Clim., 37, 249-268, https://doi.org/10.1175/JCLI-D-22-0902.sl, 2024.

Ding, Y., Cheng, X., Liu, J., Hui, F., Wang, Z., and Chen, S.: Retrieval of melt pond fraction over Arctic sea ice during 2000-2019 using an ensemble-based deep neural network, Remote Sens., 12, 2746, https://doi.org/10.3390/rs12172746, 2020.

https://doi.org/10.5194/egusphere-2026-1525
Preprint. Discussion started: 30 April 2026

Duarte, P., Sundfjord, A., Meyer, A., Hudson, S. R., Spreen, G., and Smedsrud, L. H.: Warm Atlantic Water explains observed sea ice melt rates north of Svarlbard, J. Geophys. Res. Oceans, 125, e2019JC015662, https://doi.org/10.1029/2019/JC015662, 2020.

Eicken, H., Krouse, H. R., Kadko, D., and Perovich, D. K.: Tracer studies of pathways and rates of meltwater transport through Arctic summer sea ice, J. Geophys. Res., 107(C10), 8046, https://doi.org/10.1029/2000JC000583, 2002.

Eicken, H., Grenfell, T. C., Perovich, D. K., Richter-Menge, J. A., and Frey, K.: Hydraulic controls of summer Arctic pack ice albed, J. Geophys. Res., 109, c08007, https://doi.org/10.1029/2003JC001989, 2004.

Eyring, V., Bony, S., Meehl, G. A., Senior, C. A., Stevens, B., Stouffer, R. J., and Taylor, K. E.: Overview of the Coupled Model Intercomparison Project Phase 6 (CMIP6) experimental design and organization, Geosci. Model Dev., 9, 1937–1958, https://doi.org/10.5194/gmd-9-1937-2016, 2016.

Flocco, D., Feltham, D. L., and Turner, A. K.: Incorporation of a physically based melt pond scheme into the sea ice components of a climate model, J. Geephys. Res., 115, C08012, https://doi.org/10.1029/2009JC005568, 2010.

Flocco, D., Schroeder, D., Feltham, D. L., and Hunke, E. C.: Impact of melt ponds on Arctic sea ice simulations from 1990 to 2007, J. Geophys. Res., 117, C09032, https://doi.org/10.1029/2012JC008195, 2012.

Fuchs, N., Birnbaum, G., Neckel, N., Kagel, T., Webster, M., and Wernecke, A.: Predicting melt pond coverage on Arctic sea ice from pre-melt surface topography, Geophys. Res. Lett., 52, e2025GL115033, https://doi.org/doi.org/10.1029/2025GL115033, 2025.

Hanesiak, J. M., Barber, D. G., Abreu, R. A. D., and Yackel, J. J.: Local and regional albedo observations of Arctic first-year sea ice during melt ponding, J. Geophys. Res., 106(C1), 1005–1016, https://doi.org/10.1029/1999JC000068, 2001.

Henke, M., Cassalhoa, F., Miessea, T., Ferreiraa, C. M., Zhang, J., and Ravens, T. M.: Assessment of Arctic sea ice and surface climate conditions in nine CMIP6 climate models, ARCTIC, ANTARCTIC, and ALPINE Res., 55(1), 2271592, https://doi.org/10.1080/15230430.2023.2271592, 2023.

Hersbach, H. B., Bell, P., Berrisford, G., Biavati, A., Horányi, J., Muñoz, S., Nicolas, J., Peubey, C., Radu, R., Rozum, I., Schepers, D., Simmons, A., Soci, C., Dee, D., and Thépaut, J.-N.: ERA5 hourly data on single levels from 1959 to present, Copernicus Climate Change Service (C3S) Climate Data Store (CDS), https://doi.org/10.24381/cds.adbb2d47, 2018.

Heuzé, C. and Jahn, A.: The first ice-free day in the Arctic Ocean could occur before 2030, Nature Communications, 15, 10101, https://doi.org/10.1038/s41467-024-545083, 2024.

Holland, M. N., Bailey, D. A., Briegleb, B. P., Light, B., and Hunke, E.: Improved sea ice shortwave radiation physics in CCSM4: the impact of melt ponds and aerosols on Arctic sea ice, J. Clim., 25, 1413-1430, https://doi.org/10.1175/JCLI-D-11-00078.1, 2012.

Horvat, C., Flocco, D., Jones, D. W. R., Roach, L., and Golden, K. M.: The effect of melt pond geometry on the distribution of solar energy under first-year sea ice, Geophys. Res. Lett., 47, e2019GL085956, https://doi.org/10.1029/2019GL085956, 2020.

Hunke, E. and Dukowicz, J. K.: An elastic-viscous-plastic model for sea ice dynamics, J. Phys. Oceanogr., 27, 1849-1867, https://doi.org/10.1175/1520-0485(1997)027<1849:AEVPMF>2.0.CO;2, 1997.

Hunke, E. and Lipscomb, W. H.: CICE: the Los Alamos Sea ice model documentation and software user's manual version 4.1, LA-CC-0-012, T-3 Fluid dynamics group, Los Alamos National Laboratory, Los Alamos NM 87545, 2010.

Hunke, E. C., Hebert, D. A., and Lecomte, O.: Level-ice melt ponds in the Los Alamos sea ice model, CICE, Ocean Modelling, 71, 26-42, https://doi.org/10.1016/j.ocemod.2012.11.008, 2013.

Hunke, E. C., Lipscomb, W. H., Turner, A. K., Jeffery, N., and Elliot, S.: CICE: the Los Alamos Sea Ice Model, Documentation and User's Manual Version 5.1, Los Alamos National Laboratory, USA, LA-CC-06-012, 2015.

https://doi.org/10.5194/egusphere-2026-1525
Preprint. Discussion started: 30 April 2026

Istomina, L., Heygster, G., Huntemann, M., Schwarz, P., Birnbaum, G., Scharien, R., Polashenski, C., Perovich, D., Zege, E., Malinka, A., Prikhach, A., and Katsev, I.: Melt pond fraction and spectral sea ice albedo retrieval from MERIS data – Part 1: Validation against in situ, aerial, and ship cruise data, The Cryosphere, 9, 1551-1566, https://doi.org/10.5194/tc-9-1551-2015, 2015.

Istomina, L., Niehaus, H., and Spreen, G.: Updated Arctic melt pond fraction dataset and trends 2002–2023 using ENVISAT and Sentinel-3 remote sensing data, The Cryosphere, 19, 83–105, https://doi.org/10.5194/tc-19-83-2025, 2025.

Istomina, L., M. H. H. M. H. G. and Spreen, G.: Improved cloud detection over sea ice and snow during Arctic summer using MERIS data, Atmos. Meas. Tech., 13, 6459–6472, https://doi.org/10.5194/amt-13-6459-2020, 2020.

Jahn, A., Holland, M. M., and Kay, J. E.: Projections of an ice-free Arctic Ocean, Nature Reviews Earth Environment, 5: 164-176, https://doi.org/10.1038/s43017-023-00515, 2024.

Kacimi, S. and Kwok, R.: Arctic snow depth, ice thickness, and volume from ICESat-2 and CryoSat-2: 2018–2021, Geophys. Res. Lett., 49, e2021GL097448, https://doi.org/10.1029/2021GL097, 2022.

Katlein, C., Arndt, S., Castellani, H. J. B. G., and Nicolaus, M.: Seasonal evolution of light transmission distributions through Arctic sea ice,, J. Geophys. Res.: Oceans, 124: 5418-5435, https://doi.org/10.1029/2018JC014833, 2019.

Keen, A., Blockley, E., Bailey, D. A., Debernad, J. B., Bushuk, M., Delhaye, S., Docquier, D., Feltham, D., Massonnet, F., O'Farrell, S., Ponsoni, L., Rodriguez, J. M., Schroeder, D., Swart, N., Toyoda, T., Tsujino, H., Vancoppenolle, M., and Wyser, K.: An inter-comparison of the mass budget of the Arctic sea ice in CMIP6 models, The Cryosphere, 15, 951-982, https://doi.org/10.5194/tc-15-951-2021, 2021.

Kern, S., Lavergne, T., Notz, D., and Pedersen, L. T.: Satellite passive microwave sea-ice concentration data set inter-comparison for Arctic summer conditions, The Cryosphere, https://doi.org/10.5194/tc-14-2469-2020, 2020.

Kim, Y., Min, S.-K., Gillett, N. P., Notz, D., and Malnina, E.: Observationally-constrained projections of an ice-free Arctic even under a low emission scenario, Nature Communications, 14, 3139, https://doi.org/10, .1038/s41467-023-38511-8, 2023.

Kwok, R. and Rothrock, D. A.: Decline in Arctic sea ice thickness from submarine and ICESat records: 1958–2008, Geophys. Res. Lett., 36, L15501, https://doi.org/10.1029/2009GL039035, 2009.

Lecomte, O., Fichefet, T., Vancoppenolle, M., Domine, F., Massonnet, F., Mathiot, P., Morin, S., and Barriat, P. Y.: On the formulation of snow thermal conductivity in large-scale sea ice models, J. Adv. Model. Earth Sy., 5, 542-557, https://doi.org/10.1002/jame.20039, 2013.

Lee, S., Stroeve, J., WEster, M., Fuchs, N., and Perovich, D. K.: Inter-comparison of melt pond products from optical satellite imagery, Remote Sensing of Environment, 301, 113920, 2024.

Lei, R., Tian-Kunze, X., Leppäranta, M., Wang, J., Kaleschke, L., and Zhang, Z.: Changes in summer sea ice, albedo, and portioning of surface solar radiation in the Pacific sector of Arctic Ocean during 1982–2009, J. Gerophys. Res.: Oceans, https://doi.org/10.1002/2016JC011831, 2016.

Li, Q., Zhou, C., L, L. Z., Liu, T., and Yang, X.: Monitoring evolution of melt ponds on first-year and multiyear sea ice in the Canadian Arctic Archipelago with optical satellite data, Ann. Glacio., 61(82), 154–163, https://doi.org/10.1017/aog.2020.24, 2020.

Light, B., Grenfell, T. C., and Perovich, D. K.: Transmission and absorption of solar radiation by Arctic sea ice during the melt season, J. Geophys. Res., 113, C03023, https://doi.org/10.1029/2006JC003977, 2008.

Lindsey, R. and Scott, M.: Climate change: Arctic sea ice summer minimum, https://www.climate.gov/news-features/understanding-climate/climate-change-arctic-sea-ice-summer-minimum, https://doi.org/10.25923/xyp2-vz45, 2022.

Lipscomb, W. H.: Lipscomb, W. H.: Remapping the thickness distribution in sea ice models, J. Geophys. Res.–Oceans, 106, 13,989–14,000, 2001.

https://doi.org/10.5194/egusphere-2026-1525
Preprint. Discussion started: 30 April 2026

Liu, J., Song, M., Horton, R. M., and Hu, Y.: Revisiting the potential of melt pond fraction as a predictor for the seasonal Arctic sea ice extent minimum, Environ. Res. Lett, 10, 054017, https://doi.org/10.1088/1748-9326/10/5/54017, 2015.

Maslanik, J., Stroeve, J., Fowler, C., and Emery, W.: Distribution and trends in Arctic sea ice age through spring, Geophys. Res. Lett., 38, L13502, https://doi.org/10.1029/2011GL047735, 2011.

Meier, W. N. and Stroeve, J.: An updated assessment of the changing Arctic sea ice cover, Oceanography, https://doi.org/10.5670/oceanog.2022.114, 2022.

Morassutti, M. P. and LeDrew, E. F.: Albedo and depth of melt ponds on sea ice, Int. J. Climatol., 16, 817-838, 1996.

Nghiem, S. V., Rigor, I. G., Perovich, D. K., Clemente-Colón, P., Weatherly, J. W., and Neumann, G.: Rapid reduction of Arctic perennial sea ice, Geophys. Res. Lett., https://doi.org/10.1029/2007GL03113, 2007.

Nicolaus, M., Katlein, C., Maslanik, J., and Hendricks, S.: Changes in Arctic sea ice in increasing light transmittance and absorption, Geophys. Res. Lett., 29, L24501, https://doi.org/10.1029/2012GL053738, 2012.

Nicolaus, M., Arndt, S., Katlein, C., Maslanik, J., and Hendricks, S.: Changes in Arctic sea ice result in increasing light transmittance and absorption, Geophys. Res. Lett., 39,2699-2700, https://doi.org/10.1029/2012GL053738, 2013.

Niehaus, H., Spreen, G., Istomina, L., and Nicolaus, M.: Regional and seasonal evolution of melt ponds on Arctic sea ice, The Cryosphere, 19, 2915-3938, https://doi.org/doi.org/10.5194/tc-19-3915-2025, 2025.

Notz, D. and Community, S.: Arctic sea ice in CMIP6, Geophys. Res. Lett., https://doi.org/10.1029/2019gl086749, 2020.

Peng, Z., Ding, Y., Qu, Y., Wang, M., and Li, X.: Generating a long-term spatiotemporally continuous melt pond fraction dataset for Arctic sea ice using an artificial Neural network and a statical-based temporal filter, Remote Sens., 14, 4538, https://doi.org/10.3390/rs1418538, 2022.

Perovich, D., Richter-Menge, J., and Polarshenski, C.: Observing and understanding climate change: Monitoring the mass balance, motion, and thickness of Arctic sea ice, http://imb-crrel-dartmouth.org, 2022.

Perovich, D. K. and Polashenski, C.: Albedo evolution of seasonal Arctic sea ice,, Geophys. Res. Lett., 39, L08501, https://doi.org/10.1029/2012GL051432, 2012.

Perovich, D. K., Grenfell, T. C., Light, B., and Hobbs, P. V.: Seasonal evolution of the albedo of multiyear Arctic sea ice, J. Geophys. Res., 107(C10), 8044, https://doi.org/10.1029/2000JC000438, 2002a.

Perovich, D. K., III, W. B. T., and Ligett, K. A.: Aerial observations of the evolution of ice surface conditions during summer, J. Geophys. Res., 107(C10), 8048, https://doi.org/10.1029/2000JC000449, 2002b.

Perovich, D. K., Nghiem, S. V., Markus, T., and Schweiger, A.: Seasonal evolution and interannual variability of the local solar energy absorbed by the Arctic sea ice-ocean system, J. Gerophys. Res., 112, C03005, https://doi.org/10.1029/2006JC003558, 2007.

Perovich, D. K., Richter-Menge, J. A., Jones, K. F., and Light, B.: Sunlight, water, and ice: Extreme Arctic sea ice melt during the summer of 2007, Geophys. Res. Lett., 35, L11501, https://doi.org/10.1029/2008GL034007, 2008.

Persson, P. O. G.: Onset and end of the summer melt season over sea ice: Thermal structure and surface energy perspective from SHEBA, Clim. Dyn., 39(6), 1349-1371, 2012.

Plante, M., Lemieux, J.-F., Tremblay, L. B., Tivy, A., Angnatok, J., Roy, F., Smith, G., Dupont, F., and Turner, A. K.: Using Icepack to reproduce ice mass balace buoy observations in landfast ice: improvements from the mushy-layer thermodynamics, The Cryosphere, 18, 1685-1708, https://doi.org/10.5194/tc-18-1685-2024, 2024.

Polashenski, C., Perovich, D. K., and Courville, Z.: The mechanisms of sea ice melt pond formation and evolutio, J. Geophys. Res., 117, C01001, https://doi.org/10.1029/2011JC007231, 2012.

https://doi.org/10.5194/egusphere-2026-1525
Preprint. Discussion started: 30 April 2026

Richter-Menge, J. A., Perovich, D. K., Elder, B. C., Claffey, K., Rigor, I., and Ortmeyer, M.: Ice mass-balance buoys: a tool for measuring and attributing changes in the thickness of the Arctic sea-ice cover, Ann. Glaciol., 44, 205–210, https://doi.org/10.3189/172756406781811727, 2006.

Rösel, A. and Kaleschke, L.: Comparison of different retrieval techniques for melt ponds on Arctic sea ice from Landsat and MODIS satellite data, Annal. Galcio., 52(57), 185-191, 2011.

Rösel, A., Kaleschke, L., and Birnbaum, G.: Melt ponds on Arctic sea ice determined from MODIS satellite data using an artificial neural network, The Cryosphere, 6, 431-446, https://doi.org/10.5194/tc-6-431-2012, 2012.

Rösel, A., Kaleschke, L., and Kern, S.: Gridded Melt Pond Cover Fraction on Arctic Sea Ice derived from TERRA-MODIS 8-day composite Reflectance Data bias corrected Version 02, https://www.cen.uni-hamburg.de/en/icdc/data/cryosphere/arctic-meltponds.html, World Data Center for Climate (WDCC) at DKRZ, https://doi.org/10.1594/WDCC/MODIS__Arctic__MPF_V02, 2015.

Schröder, D., Feltham, D. L., Flocco, D., and Tsamados, M.: September Arctic sea-ice minimum predicted by spring melt-pond fraction, Nat. Clim. Change, 4, https://doi.org/10.1038/NCLIMATE2203, 2014.

Seland, , Bentsen, M., Olivié, D., Toniazzo, T., Gjermundsen, A., Graff, L. S., Debernard, J. B., Gupta, A. K., He, Y.-C., Kirkevåg, A., Schwinger, J., Tjiputra, J., Aas, K., Bethke, I., Fan, Y., Griesfeller, J., Grini, A., Guo, C., Ilicak, M., Karset, I. H. H., Landgren, O., Liakka, J., Moseid, K. O., Nummelin, A., Spensberger, C., Tang, H., Zhang, Z., Heinze, C., Iversen, T., and Schulz, M.: Overview of the Norwegian Earth System Model (NorESM2) and key climate response of CMIP6 deck, historial, and scenario simulations, Geosci. Model. Dev., 13, 6165-6200, https://doi.org/10.5194/gmd-13-6165-2020,, 2020.

Serreze, M. C. and Stroeve, J. C.: Arctic sea ice trends, variability and implications for seasonal ice forecasting, Philos. Trans. Royal Soc., 373A, 20140159, https://doi.org/10.1098/rsta.2014.0159, 2015.

Spreen, G., Kaleschke, L., and G.Heygster: Sea ice remote sensing using AMSR-E 89 GHz channels, J. Geophys. Res., 113, C02S03, https://doi.org/10.1029/2005JC003384, 2008.

Steele, M., Zhang, J., and Ermold, W.: Mechanisms of summertime upper Arctic Ocean warming and the effect on sea ice melt, J. Geophys. Res., 115, C11004, https://doi.org/10.1029/2009JC005849, 2010.

Stroeve, J. C., Kattsov, V., A. Barrett, M. S., Pavlova, T., Holland, M., and Meier, W. N.: Trends in Arctic sea ice extent from CMIP5, CMIP3 and observations, Geophys. Res. Lett., 39, L16502, https://doi.org/10.1029/2012GL052676, 2012.

Tao, R., Nicolaus, M., Katlein, C., Anhaus, P., Hoppmann, M., Spreen, G., Niehaus, H., Jäkel, E., Wendisch, M., and Haas, C.: Seasonality of spectral radiative fluxes and optical properties of Arctic sea ice during the spring–summer transition, Elementa: Science of the Anthropocene, 12(1), https://doi.org/10.1525/elementa.2023.00130, 2024.

Thielke, L., Fuchs, N., Spreen, G., Tremblay, B., Birnbaum, G., Huntemann, M., Hutter, N., Itkin, P., Jutila, A., and Webster, M. A.: Preconditioning of summer melt ponds from winter sea ice surface temperature, Geophys. Res. Lett., 50, e2022GL101493, https://doi.org/10.1029/2022GL101493, 2023.

Topál, D. and Ding, Q.: Atmospheric circulation-constrained model sensitivity recalibrates Arctic climate projections, Nature Clim. Change, https://doi.org/10.1038/s41558-023-01698-1.

Tschudi, M., Meier, W. N., Stewart, J. S., Fowler, C., and Maslanik, J.: EASE-Grid Sea Ice Age, Version 4, Boulder, Colorado USA. NASA National Snow and Ice Data Center Distributed Active Archive Center, https://doi.org/doi.org/10.5067/UTAV7490FEPB, 2019.

Turner, A. K. and Hunke, E. C.: Impacts of a mushy-layer thermodynamic approach in global sea-ice simulations using the CICE sea-ice model, J. Geophys. Res. Oceans, 120, 1253–1275, https://doi.org/10.1002/2014JC010358, 2015.

https://doi.org/10.5194/egusphere-2026-1525
Preprint. Discussion started: 30 April 2026

Untersteiner, N. and Badgley, F. I.: Preliminary results of thermalbudget studies on Arctic pack ice during summer and autumn, InProceedings, Arctic Sea Ice Conference, 24–28 February 1958,Easton, MD, USA. (Publication No. 598) National ResearchCouncil, Washington, DC, 85–95, 1958.

Wang, C., Shi, L., Gerland, S., Granskog, M. A., Renner, A. H. H., Li, Z., Hansen, E., and Martma, T.: Spring sea-ice evolution in Rijpfjorden (80N), Svalbard, from in situ measurements and ice mass-balance buoy (IMB) data, Ann. Glacio., 54(62), 253-260, https://doi.org/10.3189/2013AoG62A135, 2013.

Wang, C., Graham, R. M., Wang, K., Gerland, S., and Granskog, M. A.: Comparison of ERA5 and ERA-Interim near-surface air temperature, snowfall and precipitation over Arctic sea ice: effects on sea ice thermodynamics and evolution, The Cryosphere, 13, 1661-1679, https://doi.org/10.5194/tc-13-1661-2019, 2019.

Wang, X., Liu, Y., Key, J. R., and Dworak, R.: A new perspective on four decades of changes in Arctic sea ice from satellite observations, Remote sens., 14(8), 1846, https://doi.org/10.3390/rs14081846, 2022.

Webster, M. A., Rigor, I. G., Perovich, D. K., Richter-Menge, J. A., Polashenski, C. M., and Light, B.: Seasonal evolution of melt ponds on Arctic sea ice, J. Geophys. Res.: Oceans, 120, 5968-5982, https://doi.org/10.1002/2015JC011030, 2015.

Webster, M. A., Holland, M., Wright, N. C., Hendricks, S., Hutter, N., Itkin, P., Light, B., Linhardt, F., abd I. A. Raphael, D. K. P., Smith, M. M., Albedyll, L. V., and Zhang, J.: Spatiotemporal evolution of melt ponds on Arctic sea ice: MOSAiC observations and model results, Elem. Sci. Anth., 10,1, https://doi.org/10.1525/elementa.2021.000072, 2022.

Xiong, C. and Ren, Y.: Arctic sea ice melt pond fraction in 2000-2021 derived by dynamic pixel spectral unmixing of MODIS images, ISPRS J. P RS, https://doi.org/10.1016/j.isprsjprs.2023.01.023, 2023.

Zege, E., Malinka, A., Katsev, I., Prikhach, A., Heygster, G., Istomina, L., Birnbaum, G., and Schwarz, P.: Algorithm to retrieve the melt pond fraction and the spectral albedo of Arctic summer ice from satellite optical data, Remote Sens. Environ., 163, 153-164, https://doi.org/10.1016/j.rse.2015.03.012, 2015.

Zhang, J., Schweiger, A., Webster, M., Light, B., Steele, M., Ashjian, C., Campbell, R., and Spitz, Y.: Melt pond conditions on declining Arctic sea ice over 1979-2016: Model development, validation and results, J. Geophys. Res.:Oceans, 123,7983-8003, https://doi.org/10.1029/2018JC014298, 2018.